Monopile fatigue in geographical conditions and the effect of guyed lines

MSc Offshore and Dredging Engineering

M. Saraber

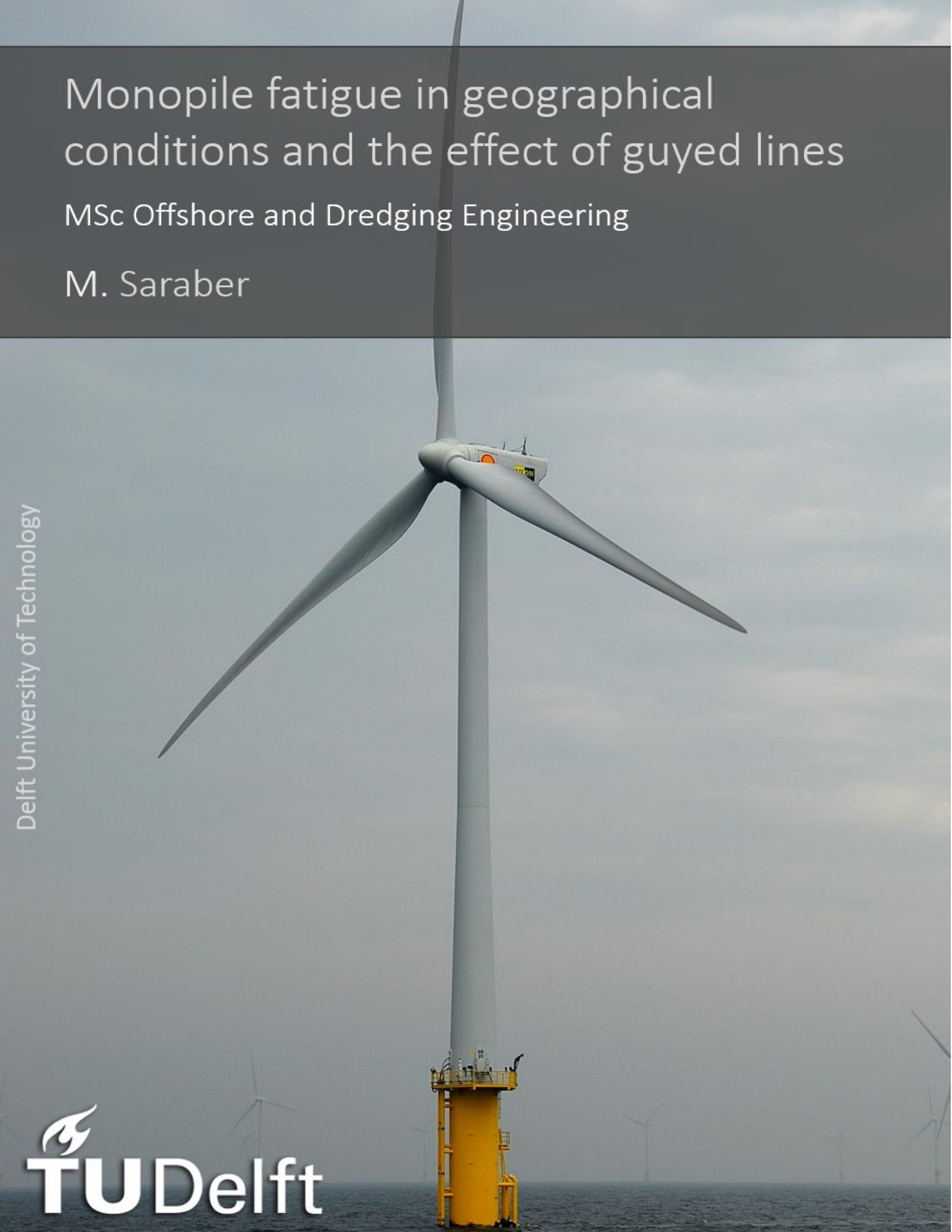

Delft University of Technology

TUDelft

Monopile fatigue in geographical conditions and the effect of adding guyed lines

Master of Science Thesis

Martijn Saraber

July 8, 2024

Student number:	4710592	
Project duration:	October 2023 – July 2024	
Faculty:	Mechanical Engineering (ME)	
Master:	Offshore & Dredging Engineering	
Thesis committee:	Ir. Andre van der Stap	TU Delft supervisor (Chairman)
	Dr.ir. Peter Meijers	TU Delft supervisor (Daily)
	Ir. Mariska van der Boon	Company supervisor

MSc Offshore & Dredging Engineering – Faculty of Mechanical Engineering (ME)

Delft University of Technology

The work in this Master Thesis was supported by Shell Global Solutions International B.V.

ACKNOWLEDGMENTS

This report presents my Master's thesis that I have worked on for the past 9 months. Not only have I learned a lot about fatigue in wind turbine foundations, but I have also thoroughly enjoyed the academic research aspect in this thesis. Throughout my thesis research, I had the privilege of working at Shell, an experienced developer in offshore projects. I am grateful for the opportunity to apply the theoretical knowledge I gained during my studies to challenges Shell is facing in the offshore wind industry. The idea that my research will contribute, even if only slightly, toward a greener future makes me proud.

I would like to extend my sincere gratitude to Andre for his feedback and critical questions during our progress meetings keeping me right on track, and for connecting me with Shell. I would also like to thank Peter for our bi-weekly one-on-one meetings which provided valuable insights throughout my thesis and guiding me to make this an academic research project. A special thanks to Mariska for her daily guidance, her always critical mindset and connecting me with the appropriate Shell colleagues for my questions. Moreover, her detailed feedback on my drafts taught me to have a more critical view and significantly improve my academic writing skills. I am also grateful to the entire Shell offshore wind department, who were always willing to assist me and engage in discussions.

Finally, I would like to thank my family, friends, and girlfriend for their invaluable support during this final stage of my study.

Martijn Saraber
Delft, July 2024

ABSTRACT

The offshore wind industry is rapidly expanding, featuring larger turbines in deeper waters and new geographical locations, leading to increased uncertainties. These developments pose significant design challenges for maintaining the simple and structural robust monopile structures, which are currently the most popular foundations for offshore wind turbines.

This study aims to investigate major contributors to fatigue on XXL monopiles supporting 15 MW and 22 MW turbines based on metocean conditions across different geographical locations. Furthermore, the impact of guyed monopiles has been analysed based on numerous water depths and soil parameters. These aspects have been largely unexplored in the existing literature.

The research uses a frequency domain monopile fatigue estimation method that integrates aerodynamic effects with hydrodynamic excitations. The method assumes a uniform wind profile and white noise wave spectrum to compute the stress response spectrum. By applying a linear correlation between the stress response spectrum and hydrodynamic excitation, the stress is determined over a wave scatter diagram, considering the joint probability of wind-wave conditions. The approach uses time series loads, computed by the aero-hydro-servo-elastic load analysis tool OpenFAST. Additionally, a dimension scaling reduction is used to reduce the mass of the monopile when incorporating the guyed lines.

The findings reveal that fatigue is dominated by scenarios lacking aerodynamic damping, such as wind-wave misalignment and idling, where directional spreading of metocean conditions has lower influence. Furthermore, fatigue damage is significantly affected by the positioning of the system's natural frequency relative to the peak wave period. A noted limitation to the model is the exclusion of turbulent wind effects.

Regarding the guyed monopile analysis, the dimension reduction strategy shows a substantial mass reduction in deeper waters. The stiffness of the system is determined by the tendon parameters, where the envelope of the natural frequency is larger in clay conditions than for sand conditions, and it increases for increasing water depth. Using a feasible tendon set-up shows higher fatigue damages at the critical location when compared with the conventional monopile fatigue damage. However, lower fatigue damages are found at other locations along the monopile length. Additionally, it is concluded that using stiff tendons results in a high risk of snap loads especially when creep of the tendon lines is considered. The results show potential for guyed monopile systems especially in deeper waters, reducing the mass, whilst maintaining similar fatigue damages as conventional monopiles. These results encourage the need for extra research on the topic of guyed monopile systems.

CONTENTS

1 INTRODUCTION

1.1 BACKGROUND

In the continuous journey of transitioning from traditional fossil fuels to clean and decarbonizing energy sources, wind energy is taking a prominent role. According to DNV [1], wind energy will play a significant role in the energy transition increasing from 750 GW of installed capacity in 2020 to 6,000 GW by 2050. It is estimated that offshore wind will significantly contribute to reaching this capacity, as the wind flows offshore are steadier, leading to higher capacity factors and limitations on land availability [2].

The foundations of offshore wind turbines can be characterized into two groups, bottom fixed and floating foundations. Floating foundations become favourable in waters deeper than 80-100 meters, as bottom fixed foundations become economically unviable [3]. However, these floaters are still in development as only small pilot projects and demonstrators are operational. Due to the complexity of floating wind turbines, bottom fixed turbines are expected to have 75% of the share of offshore wind [1].

Bottom fixed support structures include gravity-based concepts, tripods, jackets and monopiles, where the latter has the largest market share [4]. The monopile is the most popular foundation [5] as it offers manufacturing and installation simplicity, keeping the costs low, as well as having robust structural behaviour [6].

Initially, monopiles where thought to only be installed in shallow waters not exceeding 30 meters, however, offshore wind farms are moving to deeper locations [4]. Furthermore, the turbines are also increasing in capacity, therefore increasing in size [7]. Deeper waters and larger turbines lead to challenges in the design of a monopile and operation of an offshore wind turbine (OWT). Historically, the industry has designed monopile structures in the soft-stiff region. Meaning the first OWT natural frequency is placed between 1P (frequency of the rotor) and 3P (blade tower passing frequency) frequencies. In the figure below, a trend is shown of natural frequencies lowering when increasing in turbine size.

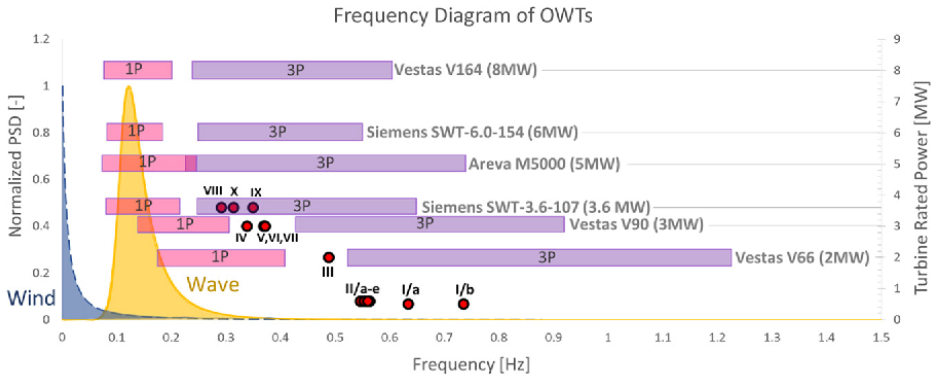

Figure 1-1: Typical wind and wave spectra, rotational speed (1P) and blade passing (3P) frequency bands for commercial turbines and measured natural frequencies of OWT (red dots) [8]

The consequence is that the natural frequencies of the larger turbines and monopiles are getting increasingly closer to the wave frequency spectrum leading to large vibrations and challenges in design.

As a result the governing limit state for XXL monopiles, here defined as monopiles with a diameter larger than 9 meters, is generally fatigue [9] [10] [11] [12]. However, due to its simplicity in fabrication and installation as well as cost effectiveness it is still expected to be the preferred foundation design when compared to jackets [13].

Consequently, due to extensive research on monopile designs, larger turbines are being installed on monopiles in deeper waters. However, the design will reach a limit due to constraints regarding fabrication, transportation and installation. Therefore, mitigations are being researched, including the implementation of tuned active mass dampers in the hub mitigating the lack of aerodynamic damping critical for fatigue damage during idling and wind-wave misalignments [14] [15] [16]. Furthermore, master thesis studies have indicated that perforated monopiles reduce wave loading on monopiles benefiting the fatigue life [17] [18]. Finally, studies have indicated a significant drop in monopile mass using guyed lines to stabilise a complaint monopile in deeper waters [19] [20] [21]. These mitigations all help increase the operational envelop of the monopile foundation, where the guyed line system has been the least intensively researched and therefore a topic investigated in this thesis.

1.2 Problem definition

Currently, the vast majority of the OWTs are operating in the southern part of the North Sea and Chinese waters. As offshore wind is becoming globally popular, more governments are auctioning off locations for offshore wind exploitation [1]. Shell is interested in these locations like the Baltic Sea, the East Coast of the United States and the central North Sea. These new locations, often in deeper waters, lead to uncertainties in feasibility of conventional monopile foundations, especially with respect to mass restrictions regarding fabrication, installation and economic feasibility.

1.3 Research objectives

The investigation of fatigue variations resulting from diverse environmental loadings has not received as much research attention compared to governing effects contributing to and methods calculating monopile fatigue. It is of strategic value for Shell to identify potential hazards and the extreme conditions a monopile can operate in, at an early stage, to reduce risks and manage difficulties. Therefore, the first research question is: ***How do different geographical regions impact the fatigue of a monopile?*** This is investigated by analysing fatigue as a result of metocean conditions from the Baltic Sea, the East Coast of the United States and the North Sea Coast of Denmark along with multiple water depths and soil conditions. The fatigue analysis involves using the 22MW and 15MW reference turbines [22] and is conducted using load outputs from the integrated load analysis (ILA) tool OpenFAST. The shear forces and bending moments estimated using the ILA tool are used as input into a frequency domain fatigue damage approximation methodology based on the work by Katsikogiannis et al. [23]. The methodology considers the joint probability of wind and wave conditions including the directionality. The reasoning behind the choices is based on literature findings documented in section 2.

Secondly, increasing the envelope of OWTs on monopile foundations using the guyed monopile system is of interest for Shell. Literature has shown that the guyed monopile system potentially reduces the monopile mass and complies with ultimate limit state requirements for structure integrity [19] [20] [21]. Mass reduction is highly beneficial as the range of installation vessels will increase along with lower material costs will lead to a decrease in costs for Shell. To the best of the author's knowledge, fatigue limit

state checks have not been documented in the literature regarding the guyed monopile system. Hence, the second research question is formulated as: ***How can guyed monopile systems help design and operate monopiles in deeper/harsher operational conditions?*** To answer this research question, an overview of the monopile mass change and gained stiffness from the tendon is given. Furthermore, a fatigue analysis is performed in line with the methodology used for the first research question. Finally, a few checks are provided analysing the total feasibility of the guyed monopile system.

1.4 THESIS OUTLINE

The opening section of this thesis is an introduction to fatigue damage on XXL monopiles and analysis methods, documented in literature. Section 3 elaborates on the wind turbine model, monopile dimension tool and the integrated load analysis tool OpenFAST used for this thesis. Thereafter, the methodology of estimating fatigue in the frequency domain is documented for the conventional monopile as well as the guyed monopile system. Sections 5, 6 and 7 show the results of the metocean hindcast data analysis, the fatigue results of the conventional monopile and the result regarding the guyed monopile respectively. The thesis is finalised by summing all the conclusions and recommending future work in section 8.

2 XXL MONOPILE FATIGUE ANALYSIS

This section provides a relevant literature background on what the author could find regarding monopile fatigue analysis during a two-month literature review period. The literature review is performed in line with a strategy documented in appendix A. Below, fatigue is discussed along with elaboration on why XXL monopiles are fatigue governing. Furthermore, published methods on calculating environmental loads as well as integrated load analysis tools are analysed. Additionally, low fidelity fatigue damage estimation methods to quickly analyse fatigue have been elaborated on. Finally, literature regarding guyed line systems has been elaborated on.

2.1 DESIGN DRIVING LIMIT STATE FOR MONOPILE

The main failure modes of an OWT support structure include fatigue, buckling, scouring, cracks in welds, excessive deflection, corrosion, vibration and fouling [24], [25]. These failure modes can be distinguished in four limit states: accidental, fatigue, serviceability and ultimate limit state, which are in accordance with the DNV guidelines [26].

The accidental limit state (ALS) considers structural damage caused by accidental loads like, excessive earthquakes or typhoons. In addition, structure collision and fire are also considered as accidental loads. The latter cases should be considered in addition to normal operational environmental conditions when accessing ALS [26].

The fatigue limit state (FLS) ensures that the design can withstand the cyclic loads for the duration of the structure's lifetime. A pile thickness and diameter are determined such that the fatigue lifetime is satisfactory. The major contributor to fatigue is structural resonance. Avoiding resonance of the structure with environmental excitations as well as mechanical excitations reduces fatigue damage [27]. Therefore, reasonable estimates are required of the systems natural frequency, which is based on the dimensions of the monopile and soil stiffness.

The serviceability limit state (SLS) requirements originate from wind turbine manufactures providing tilting restrictions for operational reasons. The recommended practice for the maximum allowable tilting angle from DNV design code [26], provides 0.25˚-0.5˚ as an order of magnitude throughout the planned lifetime. This verticality requirement originates from different design criteria, however, according to Bhattacharya et al. [28], it is mainly rooted within the onshore wind turbine sector. Furthermore, in SLS design all load cases, including extreme and accidental load should be considered as they can exceed SLS design requirement limitations.

The ultimate limit state (ULS) takes the extreme aerodynamic and hydrodynamic load cases into account. ULS considers the maximum load carrying resistance. Failure to comply to ULS results in failure of the support structure or the soil [26]. Arany et al. [27] found that when considering standard state of the art monopile designs the pile will fail first by yielding and not the soil.

Arany et al. [27] states that meeting the SLS and FLS requirements results in an over conservative design from an ULS point of view. The structure natural frequency is important from a FLS perspective. It is essential that resonance with the turbine's 1P and 3P frequency is avoided, as well as the high energy content frequency band of wind and wave excitations, to maximize fatigue life.

Regarding SLS, specific requirements are to be met, especially the tilt angle as monopiles are typically more sensitive to overturning moment rather than horizontal loading. The criteria are turbine original manufacture requirements for the operation of the turbine, which may originate from onshore wind technology. Sticking to the very low tilt angle criteria might make the design SLS dominant. This criterion however appears to be over cautious when comparing with floating OWT technology, where tilt angles up to 7˚ are deemed acceptable [29].

Concluding, literature on wind turbine reliability concludes that the design driving factor for monopiles is fatigue [9] [10]. In addition, Velarde et al. [11] and Njomo et al. [12] both concluded that fatigue is design driving for future large monopiles, as the natural frequencies of the larger OWT monopiles correspond with the peak wave spectrum frequencies. Consequently, the focus of this thesis is on fatigue driven design of XXL monopiles.

2.2 FATIGUE

Monopiles are subjected to multiple fatigue loads during their lifetime. After fabrication, large bending moments occur due to the length and the self-weight of the pile during storage and transportation. During installation the pile is excited by large hammering forces, see [30] for more information, or by axial and torsional vibrations to penetrate through the soil. Finally, after commissioning, a monopile is excited by aerodynamic and hydrodynamic forces. As the scope of this thesis is to analyse fatigue in different geographical regions, no further research has been performed on topics regarding fatigue, prior to the fully commissioned phase. In addition, the largest part of the fatigue damage of the monopile comes from operational life. DNV-ST-N001 [31] states that 10% of fatigue life is to be considered prior to operation.

2.2.1 Contributing sources to fatigue design of a monopile

The key factors determining the fatigue performance of a XXL monopile over the operational lifetime are the excitation loads, which are further elaborated upon in section 2.3.1. Additionally, damping and stiffness sources play a crucial role, which is elaborated on below.

Aerodynamic damping is the highest contributor to the overall damping mainly working in the fore-aft (FA) direction when the wind turbine is in operation and is related to the rotor speed. The aerodynamic damping during operation is variable and the levels proposed by literature vary from 2% to 8% of critical damping [32] [33]. Aerodynamic damping increases in relation to an increasing rotor speed.

Results from measurement campaigns on XXL monopiles conducted by Santos et al. [34] show that for XXL monopiles fatigue life was influenced more by hydrodynamic loading when compared to standard monopiles. The paper compared the damage in idling period and side-side (SS) direction, governed by wind-wave misalignment, of XXL monopiles compared to standard monopiles. Both cases showed significant increase in damage, as these conditions lack aerodynamic damping which has a larger impact for XXL monopiles than standard monopiles.

Horn et al. [35] solely investigated the effect of wind wave directional distribution and concluded that incorporating this in fatigue analysis reduces fatigue life. The same was found for wind-wave misalignment, shortening the fatigue life by 7 years for the cases analysed during their research. The latter can be explained because aerodynamic damping is substantial in the FA direction but almost negligible in SS direction. Hence for fatigue analysis of wind turbines and foundations, correlation between wind and wave is required.

In parked or idling conditions aerodynamic damping can almost be neglected and soil damping plays an important role [36]. Soil damping depends on the soil type and is difficult to measure directly. Different values for soil damping rations for monopiles have been suggested in literature varying from 0.17% [37] to 1.3% [38] of critical damping. The combination of hydrodynamic, structural and soil damping leads to range of 1% to 2% of critical damping according to literature [38] [39]. Hence it can be concluded that aerodynamic damping is the governing damping factor followed by soil damping.

Furthermore, soil stiffness is deemed important for the design of bottom founded support structures. Arany et al. [8] concluded that incorporating soil stiffness significantly influences the natural frequency and response of the system. Xi et al. [40] concluded that fatigue is overestimated with a 30% error when completely neglecting soil structure interaction (SSI). SSI is the response of the structure when taking both soil stiffness and damping into account. Hence, different soil profiles result in different fatigue damage.

In addition, scour protection influences stiffness, natural frequency, and hydrodynamic loading of the system [41] [42] [43]. This aspect is considered out of the scope of this master thesis as scour effects are expected to have similar effects at all locations.

2.2.2 Critical fatigue locations in monopiles

The fatigue reliability requirement is affected by the target monopile design life, typically 20-25 years [26] and inspection intervals. The fatigue assessment is usually carried out by simulating and analysing the stress at critical locations such as at the tower base [44] [45], or at the mudline [46] where fatigue damage is more pronounced in welds. Rezaei et al. [42] found the maximum bending of a 5 MW reference turbine to be 8 meters under the mudline. Thus, it is relevant to analyse several spots under mudline level to determine the weakest spot of the monopile.

2.2.3 Analysis method

Technical methods for fatigue analysis can be classified into two groups: fracture mechanics methods and S-N curve methods. In fracture mechanics, crack growth data from an initial defect of assumed geometry and size is analysed. This method involves evaluating crack growth and calculating the number of loading cycles needed for initial defects developing into cracks large enough to trigger fracture [47]. The S-N curve method requires the use of fatigue test data to analyse the fatigue of a structure. Due to its convenient implementation and high reliability, the S-N curve approach is recommended by the current international design standard of wind turbines [48]. Therefore, the S-N curve method is used for fatigue analysis in this thesis. For more elaboration on the fracture mechanics method and its application in offshore wind turbine fatigue analysis, reference is made to [49] [50] [51].

The S-N data is obtained from fatigue tests which is analysed to obtain S-N curves and associated parameters A and slope m. These parameters depend on material types, environmental conditions and whether to use cathodic protection. For offshore steel structures, DNVGL-RPC-203 [52] C, C1 and D curves are commonly used [53] [54]. It should be noted that the S-N curves stated in the DNVGL-RPC-203 [52] are now several years old and originate from the Oil and Gas industry. This industry fundamentally differs from structures in the wind industry in terms of load regimes, environment and structural characteristics. However, as these curves are still used in common practice for fatigue assessment of offshore wind turbines, characteristics from the S-N curves have been used in this thesis.

Along with the S-N curves, Miner's rule [55] has been widely used in fatigue assessment of OWT structures [53] [56]. Miner's rule [55], based on the linear damage hypothesis is extensively used as cumulative

damage model for fatigue failures. The amount of stress cycles is counted and linearly compared to the average number of cycles to failure for a certain stress range coming from the S-N curve.

To determine the number of cycles from a variable amplitude loading history, a cycle counting method is required. Literature has proposed a variety of methods, including simple range counting, level crossing counting, peak counting, mean crossing peak counting and rainflow counting [57]. Different counting methods give different results for the same strain history. The rainflow counting method has demonstrated good agreement with measured fatigue lives [58], making it the most common counting method used in the offshore structure design [11] [53].

Concluding, using DNVGL-RPC-203 [52] S-N curves along with Miner's rule [55] using a form of rainflow counting method is the most common method used for fatigue analysis.

2.2.4 Uncertainties of sources for fatigue design of a monopile during operation

Fatigue calculation uncertainties are well documented in the literature. The main contributors to uncertainties in fatigue calculation results are choices in turbulence intensity and wave directionality (short and long crested waves). For further reading on fatigue reliability and contributing factors, reference is made to literature [9] [59].

Uncertainties are considered outside the scope of this master thesis as the goal is to give an indication of differences in fatigue damage in different geographical regions. As the same fatigue calculation method will be used for each geographical location, the uncertainties associated with the results will be similar.

2.3 LOAD ANALYSIS

The scope of this thesis is focused on fatigue limit state, which is governed by cyclic loading from wind (aerodynamic loads) and waves (hydrodynamic loads).

2.3.1 Loads

Aerodynamic loading on an OWT structure is caused by wind. The aerodynamic loading can be split into two components, thrust and drag. Thrust force solely acts on the rotor and drag forces act all over the OWT subjected to wind. Three approaches shown in Figure 2-1 are commonly used to calculate the aerodynamic loads on a wind turbine, namely Blade Element Momentum (BEM), Generalised Dynamic Wake (GDW), and Computational Fluid Dynamics (CFD). BEM has the highest calculation efficiency and gets satisfactory results, when considering total loading on OWT support structures [60]. Therefore, BEM is most widely used method in the industrial practice for the calculation of aerodynamic loads [61].

The classical BEM method is based on steady flow [62] hence, neglecting wind turbulence. However, Sørum et al. [59] indicated in their research that turbulence intensity impacts fatigue damage. The unsteady BEM theory [62] [63] accounts for turbulent flows and wind shear effect. Furthermore, the classical BEM method assumes no interaction between blade elements at different radial positions and it does not account for wake expansion and tip losses [62]. To account for this, corrections on the classical BEM method, which include Prandtl tip loss, Glauert induction and dynamic stall and wake, must be applied. Software tools analysed for this thesis in section 2.3.2 all include these corrections when calculating aerodynamic loading with the BEM method.

Hydrodynamic loading, on an OWT support structure, is caused by waves and currents. As with aerodynamic loading there are different fidelity models as shown in Figure 2-1. Because of its simplicity

and applicability for cylindrical structures, the Morison's equation [64], along with MacCamy and Fuchs correction [65] for diffraction, is the most widely used in commercial software to model hydrodynamic loads for large diameter piles [66]. Furthermore, choices on wave models influence the excitation. Ning et al. [67] concluded that second order solutions are very close to fully nonlinear solutions when comparing first order, second order and fully nonlinear solution. Chen et al. [68] show that wave models on a monopile in third and fourth order have lower impact than the second order component.

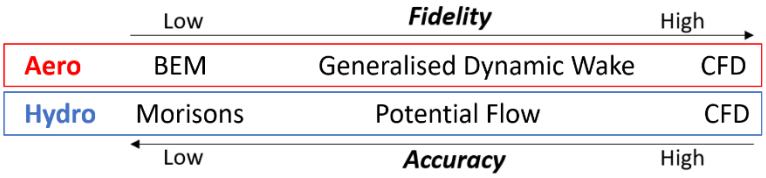

Figure 2-1: Overview of computational effort and accuracy of aerodynamic and hydrodynamic modelling choices

Therefore, it is currently preferred to use BEM with the appropriate corrections for the aerodynamic loading coupled with Morison's equations along with 2nd order waves to represent hydrodynamic loading, for fatigue analysis.

2.3.2 Integrated load analysis (ILA) tools

Research institutions, the industry and universities have been working on the creation and development of models to accurately predict the coupled dynamic loads and response of OWT's. For this thesis five industry used software models have been compared. The five considered are, BLADED [69], HAWC2 [70], OpenFAST [71], OrcaFlex [72] and 3DFloat [73]. An overview of the specifications of these tools is given in Table 2-1.

Table 2-1:Overview of aero-hydro-elastic modelling capabilities adapted from [74] and [66]

Developer	Code	Aerodynamics	Hydrodynamics	Structural dynamics
DNV	BLADED	(BEM or GDW) + DS	Linear airy + ME	MBD
DTU	HAWC2	(BEM or GDW) + DS	Linear airy + ME	MBD/FEM
NREL	OpenFAST	(BEM or GDW) + DS	2nd O-S + ME	FEM + (Modal/MBD)
Orcina	OrcaFlex	(BEM or GDW) + DS	FNPF + ME	MBD
IFE	3DFloat	(BEM or GDW) + DS	FNPF + ME	MBD
	BEM: blade element momentum **GDW:** generalized dynamic wake **DS:** dynamic stall **ME:** Morisons equation		**O-S:** order Stokes **FNPF:** fully nonlinear potential flow **MBD:** multi body dynamics **FEM:** finite element method	

These models were compared against each other in Offshore Code Comparison Collaboration OC3 for International Energy Agency (IEA) and the hydrodynamic component was compared to test results in OC5. As shown in Table 2-1 the aerodynamic and structure dynamic modelling approaches do not vary per code, where the hydrodynamic modelling approaches vary significantly. In OC5 [66] it is concluded that the software developed by NREL, Orcina and IFE had the best correlation with the test results. As the tool developed by NREL is open source, Shell doesn't require a license for the tool. In addition, OpenFAST includes aerodynamic and hydrodynamic corrections mentioned in section 2.3.1. Therefore, for this thesis OpenFAST is used as ILA tool.

2.4 LOW FIDELITY FATIGUE DAMAGE ESTIMATION METHODS

According to DNV-ST-0126 [26], fatigue assessment is based on fully integrated time domain simulation, which is a time consuming process. The conditions that should be considered include the joint occurrence of wind speed, significant wave height, wave peak period and wind-wave directionality. For a full fatigue analysis, an ILA analysis in accordance with section 2.3 to determine the loads is preferred. In addition, rainflow counting along with DNVGL-RPC-203 [52] S-N curves and Miner's rule [55] is used to determine the short term damage analysis as concluded in section 2.2.3. This is the most common used approach for fatigue analysis and is visualised in Figure 2-2.

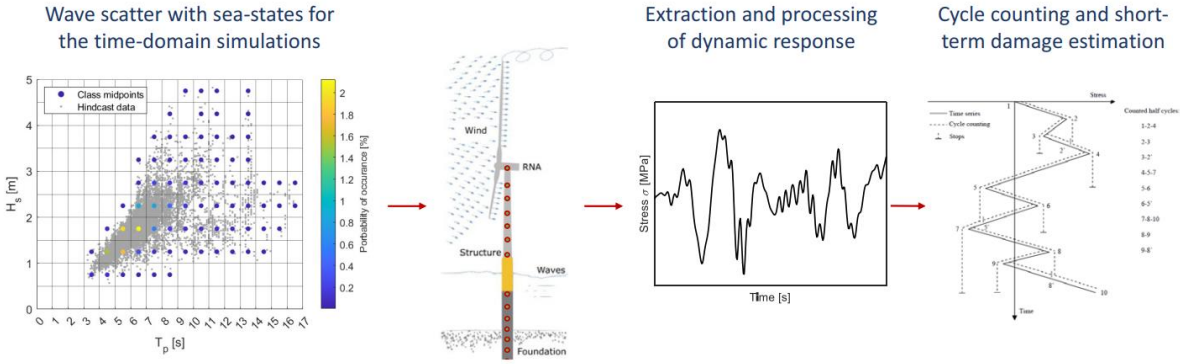

Figure 2-2: Time domain procedure to estimate short term damage fatigue for each sea state in a wave scatter diagram [23]

Reducing the computational time is beneficial for the fatigue damage analysis considering multiple input parameters. The challenge however is accurately predicting the fatigue damage whilst lowering the computational time. To the best of the author's knowledge there are four low fidelity methods documented in the literature regarding fatigue analysis.

First, a probabilistic approach, only considering the highest probable occurring sea-state from a scatter diagram (SCD) and using these lumped load conditions for a full time domain ILA analysis above. This method is based on the method used in the oil and gas industry. Second, approach is an iterative damage equivalent approach according to Kühn [75]. Third, Seidel [76] developed a damage equivalent approach in the frequency domain. Finally, Passon [77] built a frequency domain lumping method establishing wind-wave correlations which is crucial for fatigue design. Katsikogiannis et al. [23] incorporated operational effects in Passon's method.

All these approaches reduce the computational time in determining the fatigue whilst correlating wind and wave parameters. Reducing computational time contributes significantly to the early design phase of the OWT support structure, as fatigue issues can be discovered early.

The approaches in Kühn [75], Seidel [76] and Passon [77] only incorporate hydrodynamic loading, completely neglecting aerodynamic loading and aerodynamic damping. Disregarding these aspects corresponds to non-operational conditions which occur typically 10% of the operational lifetime [26]. Furthermore, as mentioned in 2.2.1 aerodynamic damping is favourable for fatigue life and therefore neglecting this results in conservative fatigue estimations. Hence it is of importance to include the aerodynamic effects of the system.

Katsikogiannis et al. [23] have developed a frequency domain method considering aerodynamic effects during operation to determine the fatigue damage. The method is verified using integrated load time domain simulations of the whole scatter diagram. The results obtained from the frequency domain lumping method are deemed to be in reasonable comparisons, 10% deviation, with the fully integrated time domain scatter diagram analysis.

Concluding, Katsikogiannis et al.'s [23] method, integrating aerodynamic effects into a frequency domain fatigue analysis, demonstrating reasonable results compared to fully integrated time domain simulations, serves as the foundation of this thesis.

2.5 MONOPILE GUYED LINE SYSTEM

Above, relevant literature on loads and fatigue calculations is elaborated on, providing background for research question 1. The second scope is to analyse the effect of connecting guyed lines on a monopile to increase the envelope of the simple monopile structures.

Guyed masts have been applied within the field of telecommunications for many years and research has also been published on guyed wind turbine towers for onshore applications [21]. Both applications highlight positive properties, like lower mass with increasing height and cost-effective foundations. However, little literature has been published on guyed monopile systems.

Connecting guyed lines on a monopile changes the structural properties of the OWT system by increasing stiffness and stability. The tendons are anchored to the seabed and can be pretensioned to 20-45% of their minimum breaking load [21]. The guyed lines transfer a significant part of the wind and wave excitation loads directly to the soil, decreasing the bending moments and shear stresses in the monopile [20]. As a result, the monopile can be designed with smaller diameters and wall thicknesses. Material properties and pretension of the tendons influence the magnitude of the bending moments in the monopile along with the natural frequency of the system [20] [21].

Both [19] [20], performed structural analysis on the offshore application of guyed monopile systems and show positive results regarding mass reductions whilst complying with ULS and SLS standards. A detailed column buckling, and local buckling analysis was performed by Van Doormaal [19] showing positive results with respect to bucking failure. However, to the best of the author's knowledge, no fatigue analysis has been documented in the literature. Additionally, the effect of tendon stiffness and configuration on the natural frequency of the guyed monopile system have not been published. Finally, a mode shape comparison with conventional monopiles has not be documented in literature.

3 NUMERICAL MODEL

In this thesis, OpenFAST is used as integrated load analysis (ILA) tool. In addition, opensource offshore wind turbines (OWTs), section 3.1, are used as input and monopile designs, section 3.2, are derived from a preliminary monopile design tool.

3.1 WIND TURBINE MODELS

As input turbine for the OpenFAST model opensource OWTs are used. Two turbines and corresponding turbine towers have been selected for this thesis to research the effect of guyed lines on bigger turbines. Both are developed by International Energy Agency (IEA), under IEA Wind TCP Task 37, for research purposes. The main parameters of the turbines are given in Table 3-1.

Table 3-1: Main parameters of the OWTs used for this thesis

Parameter	Unit	IEA 15 MW	IEA 22 MW
Power rating	MW	15	22
Rotor orientation	-	Upwind	Upwind
Number of blades	-	3	3
Cut-in wind speed	m/s	3	3
Rated wind speed	m/s	10.5	11
Cut-out wind speed	m/s	25	25
Minimum rotor speed	RPM	5	2.0
Rated rotor speed	RPM	7.56	7.2
Maximum tip speed	m/s	95	105
Design tip speed ratio	-	9	9.2
Hub height	m	150	170
Hub diameter	m	7.9	8.4
Rotor diameter	m	242	283
RNA mass	ton	950	1200
Tower base diameter	m	10	10

3.2 CONVENTIONAL MONOPILE

Monopiles are used as foundation for the WTG. As the goal of this thesis is to research the effect of water depth, soil parameters and metocean conditions of a conventional monopile on fatigue, different monopile designs are required. The monopiles designs are computed using an initial monopile optimisation tool.

In this thesis, OWT, water depth and soil parameters are the main parameters which have been used as input for monopile design.

In Table 3-2 and Table 3-3 main parameters of the monopile design are shown. In these tables m represents mass, D_{bottom} is the bottom diameter, L is the length and ω_n is the natural frequency.

Throughout the thesis, all monopiles are designed to have an interface level of 15 meters above mean sea level (MSL).

Table 3-2: Main parameters of the 15 MW monopiles used for this thesis

		40m water depth		**60m water depth**		**80m water depth**	
Parameter	**Unit**	*Clay*	*Sand*	*Clay*	*Sand*	*Clay*	*Sand*
m	ton	2,091	1,595	3,956	2,564	5,359	4,037
D_{bottom}	m	10.0	10.0	10.9	12.0	14.8	14.3
L	m	94.6	84.1	124.9	110.1	150.7	136.9
ω_n	hz	0.170	0.181	0.166	0.180	0.175	0.179

Table 3-3: Main parameters of the 22 MW monopiles used for this thesis

		40m water depth		**60m water depth**		**80m water depth**	
Parameter	**Unit**	*Clay*	*Sand*	*Clay*	*Sand*	*Clay*	*Sand*
m	ton	2,556	1,916	4,334	3,221	6,666	5,184
D_{bottom}	m	11.6	11.2	13.5	13.3	14.1	15.3
L	m	99.8	87.6	128.0	113.9	155.4	139.9
ω_n	hz	0.137	0.142	0.136	0.141	0.130	0.138

3.3 OpenFAST

OpenFAST V3.5.0 is used as ILA tool. It is a fully coupled multi body dynamics (MBD) software, coupling aerodynamic, hydrodynamic, structural dynamic and control systems. A schematic block diagram is given in Figure 3-1, providing an overview of the coupling in OpenFAST.

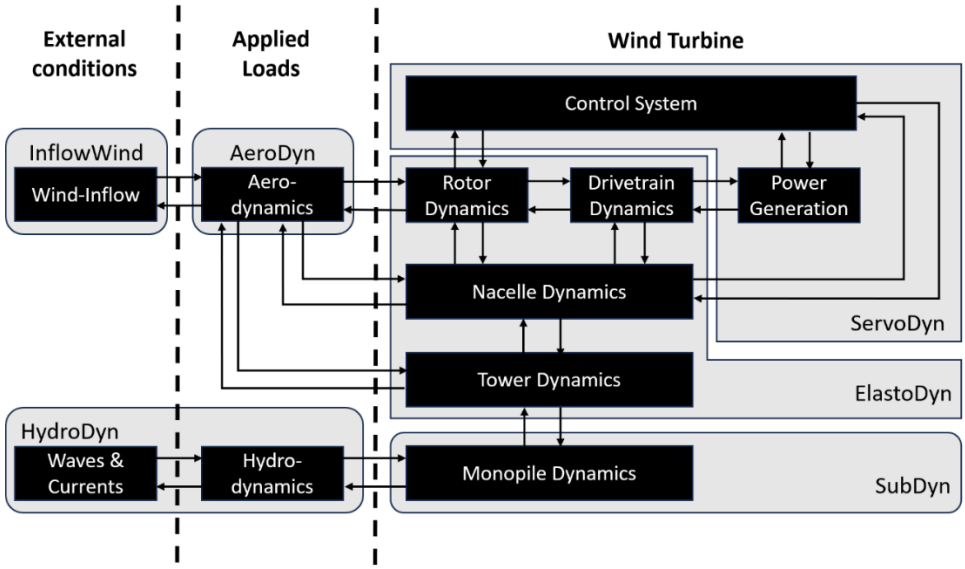

Figure 3-1: Overview of OpenFAST v3.5.0 coupling of modules for bottom founded structures

As shown in Figure 3-1, OpenFAST has many modules. For the purpose of this thesis, the focus is put on the modules AeroDyn, HydroDyn and SubDyn. For the control module ServoDyn, the ROSCO V2.9.0 controller is used, which is commonly used default controller.

3.3.1 Aerodynamic

For the Aerodynamic modelling, the AeroDyn-15 module is used in OpenFAST. This module calculates the aerodynamic loads on both the tower and blades of the OWT allowing for aero-elastic simulations using an actuator line model. The loads are dependent on the properties of the OWT documented in section 3.1.

The AeroDyn module uses quasi-steady Blade Element Momentum (BEM) theory to calculate the loads and influence of wake. For high axial induction factors Glauert's empirical correction is used to replace the linear momentum balance. Furthermore, Prandtl corrections for tip and hub losses have been applied in the model.

3.3.2 Hydrodynamic

The Morison's equation serves as the basis for the hydrodynamic model in OpenFAST and is recommended in standards as mentioned in section 2.3. The equation is semi-empirical and assumes that the cylinder is slender, meaning the diameter is small compared to the wavelength. This assumption implies that the cylinder does not significantly generate a diffracted wave field. Morisons equation combines a viscous drag component and an inertia component and is formulated as follows:

$$dF = \frac{1}{2} C_d \rho D |u - v|(u - v) + C_m \rho \frac{\pi}{4} D^2 (\dot{u} - \dot{v}) - \rho \frac{\pi}{4} D^2 \dot{v}$$

Here, dF is the force per unit length, C_d, C_m are the drag and inertia coefficients respectively, ρ is the water density, D is the monopile diameter, u, $\dot{u}$ are the horizontal water velocity and acceleration and v, $\dot{v}$ are the structural velocity and accelerations. The force is dependent on the geometry of the monopile, which is documented in section 3.2.

The drag and inertia coefficients, C_d and C_m vary with different parameters such as Reynolds number, Keulegan-Carpenter number, surface roughness and ratio of current or wave velocity to the cylinder velocity. Studies have shown significant variations in these coefficients however, for design calculations in accordance with DNVGL-RP-C205 [78], it is common practice to assume constant values of 0.9 and 2.0 for the drag and inertia coefficient respectively.

For dimensions of structures that are large compared to the incident wave wavelength λ, typically when $D > 0.2\lambda$, diffraction effects are of relevance. For these instances Morisons equation is no longer sufficient. DNVGL-RP-C205 [78] recommends using MacCamy and Fuchs [65] solution for the diffraction of long waves on vertical piles. Morisons equation can still be used for the drag term. However, the inertia term varies depending on the size of the pile and the frequency of the incoming waves.

OpenFAST V3.5.0 does not allow the use of the MacCamy and Fuchs solution in the HydroDyn module and is therefore not implemented in this thesis. However, as the purpose of this thesis is to identify trends in different parameters the results obtained can be used for further studies.

OpenFAST V4.0 incorporates the MacCamy and Fuchs solution in a new module named SeaState. However, OpenFAST V4.0 is still in a test phase at the time of this research therefore, not used in this

thesis as it is seen as unstable. In section 4.2.4.3 results including the MacCamy and Fuchs diffraction relation are compared with results neglecting the diffraction effect.

3.3.3 Soil

This thesis distinguishes two soil profiles, namely dense sand and stiff clay. The soil properties are listed in Table 3-4.

Table 3-4: Soil properties

Description	**Thickness** [m]	**Unit Weight** [kN/m3]	**Unit weight subm.** [kN/m3]	**Friction angle** [degree]	**Undrained shear strength** [kpa]	ϵ_{50}
Dense Sand	80	20.0	10	39	-	-
Stiff Clay	80	17.5	7.5	-	100	0.01

OpenFAST V3.5.0 does not include a soil module, which is included in OpenFAST V4.0. The result is that the author is not able to model springs and dampers imitating the soil behaviour in OpenFAST V3.5.0. However, soil conditions do influence the fatigue damage as concluded in section 2.2.1. Table 3-2 and Table 3-3 both show differences in natural frequencies between monopiles in sand conditions and clay conditions.

To model this structural behaviour, the soil is modelled using the effective fixity length strategy. The monopile dimensions from initial monopile design tool are used in the SubDyn module and fixed at the bottom of the monopile below the mudline. The first natural frequency of this system is analysed, after which, the length of monopiles fixed embedded length is tuned accordingly. A shorter fixed embedment length results in a higher natural frequency and a longer fixed embedment length vice versa. The strategy is visualised in Figure 3-2.

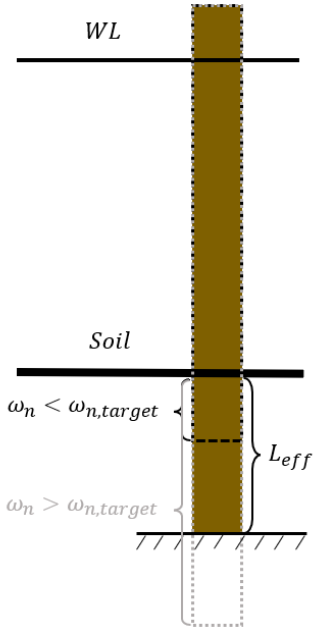

Figure 3-2: Schematic overview of tuning natural frequency using effective fixity length strategy

3.3.4 Outputs numerical model

OpenFAST V3.5.0 generates time domain outputs of environmental inputs and displacements and forces thoughout the system. For this thesis, general outputs used are wave elevation, forces F_x, F_y, F_z and moments M_x, M_y, M_z at critical locations of the monopile in time domain.

3.4 Implementation of guyed lines in model

The implementation of the guyed lines is performed in the OpenFAST SubDyn module. For the base case, it is assumed that the guyed line system will consist of 3 tendons evenly spaced around the monopile. Furthermore, the tendons are connected to the monopile node at 10 meters below MSL at a 45 degree angle relative to the monopile. It is chosen to fix the guyed lines at 10 meters below MSL. Figure 3-3 visualizes the description above.

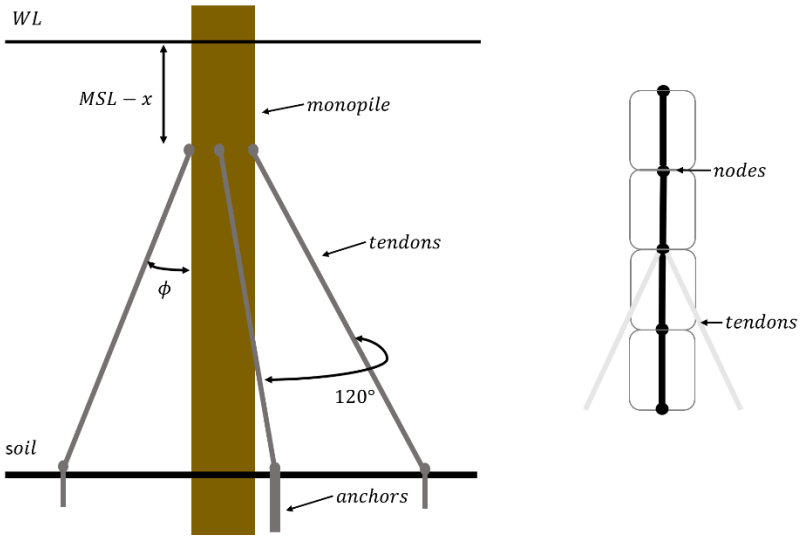

Figure 3-3: A schematic overview of guyed monopile model and fixed parameters (left) and a schematic visualization of how the tendons have been modelled in OpenFAST on the monopile (right)

The variable parameter chosen in this thesis is the stiffness of the tendon. The SubDyn module enables users to specify cable properties, which will be used as the tendon properties for this thesis. OpenFAST uses a stick model for modelling, where the user can determine the location of the nodes, for the monopile foundation visualised in Figure 3-3. By connecting the cable to the monopile node at 10 meters below MSL and seabed node, the tendon is modelled. Input parameters for the cables section in OpenFAST are the elasticity modulus multiplied by area, EA in (N), the material density in (kg/m), and the initial tension T_0 in (N).

To calculate the stiffness of these lines the following relation is used.

$$k = \frac{EA}{L_0}$$

Here, EA are the elasticity modulus and area of the cable, which are input parameters and L_0 is the initial length of the cable. The initial length can be related to the length of the cable under tension, L_e, using equation.

$$L_0 = \frac{L_e}{1 + \epsilon_0}$$

And

$$\epsilon_0 = \frac{T_0}{EA}$$

Where, T_0 is the initial tension, which is the final input parameter.

Due to the underlying linear spring theory in the SubDyn module, the stiffness of the tendon line will apply in both tension and compression. However, in reality the tendon line stiffness only works at tension. This should be considered when analysing the results. Furthermore, it is assumed that the tendon cannot transmit bending moments, which aligns with the assumptions in the underlying SubDyn module. Finally, the SubDyn module can model the tendons only using cantilever joints.

In this thesis, the effect of the tendon stiffness will be analysed, though a parametric study that analyses numerous stiffness values.

4 FATIGUE DAMAGE CALCULATION METHODOLOGY

For fatigue analysis of an OWT, the conventional approach is to analyse all sea states with a non-zero probability of occurrence in the wave scatter diagrams as suggested by the design standard DNVGL-RP-C205 [78]. To estimate the short-term fatigue damage for each sea state in the scatter diagram the time domain of the stress is analysed as documented in section 2.4. The long-term damage is determined by multiplying the probability of occurrence and the design life of the structure, which is based on the Palgrem-Miners linear damage hypothesis.

The procedure described above is a full long-term time domain fatigue assessment. This procedure requires the analysis of many load cases resulting in a high computation time and is often only performed for final monopile designs.

As the objective of this thesis is to perform fatigue analysis on monopiles in different water depths, soil conditions, geographical regions and compare with a guyed monopile system, a more efficient analysis methodology is required. Firstly, in this research, a metocean data analysis consisting of a joint probability distribution with satisfactory bin sizes is performed in accordance with section 4.1. This metocean analysis forms the basis of the fatigue domain analysis methodology documented in section 4.2. This frequency domain approach is checked using full time domain fatigue assessments as previously described in section 4.2.4. Finally, this process is repeated for the implementation of the guyed line system, section 4.3.

For the fatigue analysis of the conventional monopile design the mudline is chosen as the weakest location. Section 2.2.2, concluded that the critical location is just below mudline, however, as mentioned in section 3.3.3, OpenFAST V3.5.0 is unable to model the soil as springs and therefore, no reaction force can be determined below mudline. Hence, for consistency across all water depths and soil parameters considered, the mudline is used as the critical location for the fatigue analysis of conventional monopiles. Analysis is performed on the moment line for the guyed monopile system. The analysis fatigue analysis is performed at the location of the largest moment, whether it's the connection point or mudline. Figure 4-1 gives an overview of the methodology and how the inputs of the numerical model and results relate to the methodology.

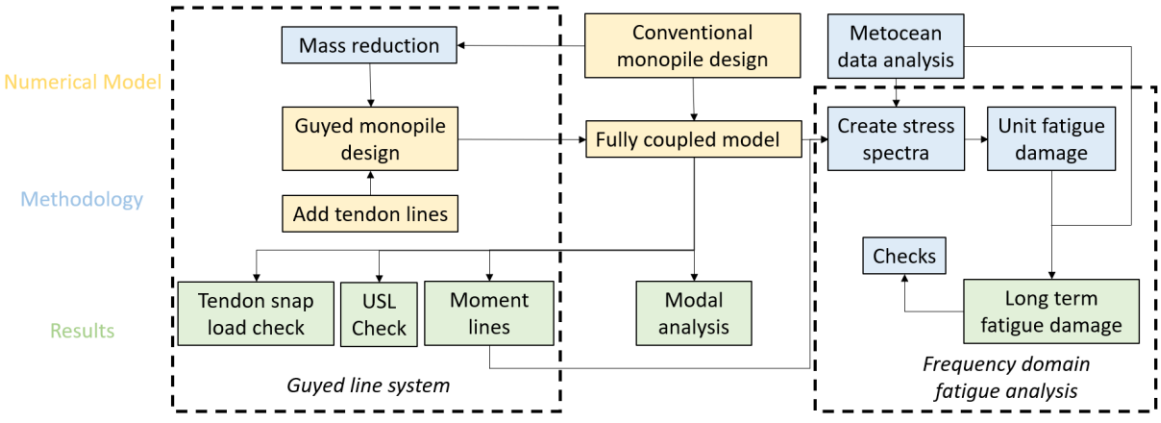

Figure 4-1: Block scheme on the relation of the contents of the numerical model, the fatigue methodology and results are related

4.1 Environmental bin method and probability of occurrence

For the analysis of fatigue in this thesis, environmental conditions in the operational wind speeds of the turbines introduced in section 3.1 is considered. This assumption is deemed valid, as for all three locations analysed in section 5 the environmental conditions during operational wind speeds have a probability of occurrence over 90%. Hence, fatigue is analysed for wind speeds in the range $3 - 25$ m/s throughout this research.

Efficiently binning the environmental load is essential for an accurate fatigue analysis. Large bins lead to lower computational time but yield inaccurate results. Too small bins give accurate results however but lead to higher computational times. Studies, [79] [80] have been performed to find efficient bin sizes for the fatigue analysis of offshore wind. The bin sizes in this thesis are documented in Table 4-1 and are in accordance with these studies.

Table 4-1: Overview of bin sizes. H_s and T_p represents the significant wave height and the peak period respectively, U_w the wind speed, θ_{wi} and θ_{wa} the wind and wave directionality.

Parameter	H_s	T_p	U_w	θ_{wi}	θ_{wa}
Bin size	0.5 m	1 s	2 m/s	30°	30°

Furthermore, for long term fatigue damage assessment of OWTs wind-wave correlation and directionality assessment is required. It is assumed that the joint probability of all environmental parameters can be expressed as the product of marginal and conditional probabilities. In addition, the wave direction is implicitly modelled by the wind-wave misalignment $\theta_{rel} = \theta_{wi} - \theta_{wa}$, giving the following probability distribution [80].

$$P\{U_w, \theta_{wi}, \theta_{rel}, H_s, T_p\} = P\{U_w\}P\{\theta_{wi}|U_w\}P\{\theta_{rel}|U_w\}P\{H_s, T_p|U_w, \theta_{rel}\}$$

4.2 Fatigue estimate in frequency domain method

For the fatigue assessment in frequency domain, a method based on the frequency domain approach developed by Katsikogiannis et al.'s [23] is used. This method uses both hydrodynamic effects as well as aerodynamic effects during operation, mentioned in section 3.3. Katsikogiannis developed the frequency domain methodology to determine the lumped loads using a damage equivalent approach. In this thesis, the method is solely used to determine the fatigue damage of the monopile.

The fatigue methodology consists of three main steps. The first step is to derive the stress spectrum along the support structure for each sea state. The second step involves determining the spectral unit fatigue damage. The final step is to determine the long-term fatigue damage using the Palgrem-Miners linear damage hypothesis which is added to the Katsikogiannis's method.

4.2.1 Derivation of the spectra

To derive the stress spectrum using OpenFAST as a fully coupling model, a white noise wave excitation and uniform wind are applied to the OWT model for each wind class. The uniform wind speed neglects turbulence and wind shear which linearises the model. The white noise wave contains frequencies in the range $10^{-3} - 1$ hz capturing all possible wave frequencies. For each wind class, $U_{w,k}$, the most probable H_s value is used to determine the magnitude of the white noise wave. In this thesis, one realisation of the 1 hour time domain wave elevation derived from the white noise wave spectrum is used. Hence, only one

seed is considered, assuming stationary environmental conditions. A further assumption is to neglect current, which is not a major factor in fatigue as this is a constant force.

By conducting time domain simulations from the white noise wave input, the time domain forces and moments are obtained in OpenFAST. Using the following equation, the time domain stress response can be obtained.

$$\sigma_x(\phi) = \frac{F_x}{A} - \frac{M_y}{I_y} r sin(\phi) + \frac{M_z}{I_z} r cos(\phi)$$

In the equation above, σ_x is the axial stress, F_x, M_y, M_z are the gravitational force, and bending moments respectively, A is the area of the monopile, I_y, I_z are the area moments of the monopile, r is the radius of the monopile and ϕ is the angle of the node on the monopile. Only axial stress is considered in this thesis as this is dominant when compared to shear stress.

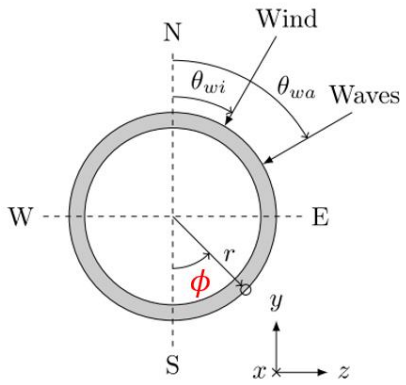

Figure 4-2: Monopile cross section local coordinate system and environmental parameters

To compute the frequency domain of these time domain stress signals, the Fast Fourier Transform (FFT) is used. The FFT computes a two-sided magnitude signal. The two-sided spectrum is converted into a one sided magnitude spectrum by multiplying the magnitude by two in the frequency range $0 - F_n$ hz, where F_n is the Nyquist frequency. Finally, the magnitude spectrum is converted into a power spectral density spectrum using the following relation.

$$S_X(f) = \frac{1}{2\Delta f} \hat{X}^2$$

Here, Δf is the sampling frequency and $\hat{X}$ is the magnitude spectrum.

Then, by assuming a linear relationship between the stress response and the wave elevation the following transfer function can be obtained.

$$\left|H_{\sigma,\zeta}(f)\right| = \sqrt{\frac{S_\sigma(f)}{S_\zeta(f)}}$$

Where S_σ and S_ζ are the spectral densities of stress and wave respectively. This transfer function represents the spectral relationship between wave elevation and stress for a given wind class.

Figure 4-3 gives an overview of the procedure to derive the stress transfer function for a wind class.

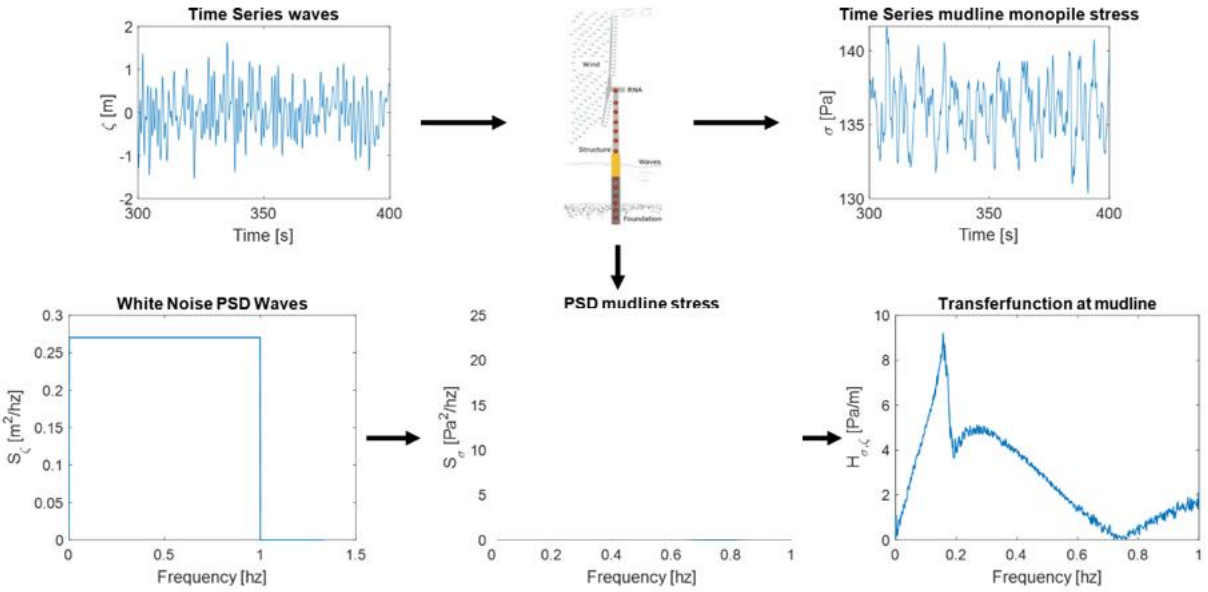

Figure 4-3: Overview of determining the transfer function associated with a wind speed class (10-12 m/s) using a fully integrated time domain model

The transfer functions $H_{\sigma,\zeta}(f)$ obtained for each wind class is combined with a typical JONSWAP wave spectra corresponding to each $H_{s,i} - T_{p,j}$ bin resulting in a representative stress spectrum, $S_{\sigma,i,j}(f)$ in the wave scatter diagram. This stress spectrum represents the dynamic excitations caused by the waves along with the mean thrust force and aerodynamic damping. The aerodynamic excitation caused by tower shadow and blade passing frequencies is added to the stress spectra $S_{\sigma,i,j}(f)$ using the same change in magnitude at the frequencies which was filtered out of the stress response spectrum above. It is therefore, assumed the aerodynamic excitation has the same magnitude for all sea states. The procedure to derive the stress spectrum $S_{\sigma,i,j}(f)$ is visualised in figure Figure 4-4.

4.2.2 Spectral unit fatigue damage

For the estimation of the unit fatigue damage for an environmental condition $H_{s,i} - T_{p,j}$ in the wave scatter diagram associated with a wind class $U_{w,k}$, the derived stress spectrum $S_{\sigma,i,j}(f)$ is used. The unit fatigue damage represents the short-term damage over a specified period, like 1 hour. The calculations for this method are based on the book Dynamics of Fixed Marine Structures [81].

An irregularity factor β is determined based on the stress spectrum as follows.

$$\beta = \left(\frac{m_2^2}{m_0 m_4}\right)^{1/2}$$

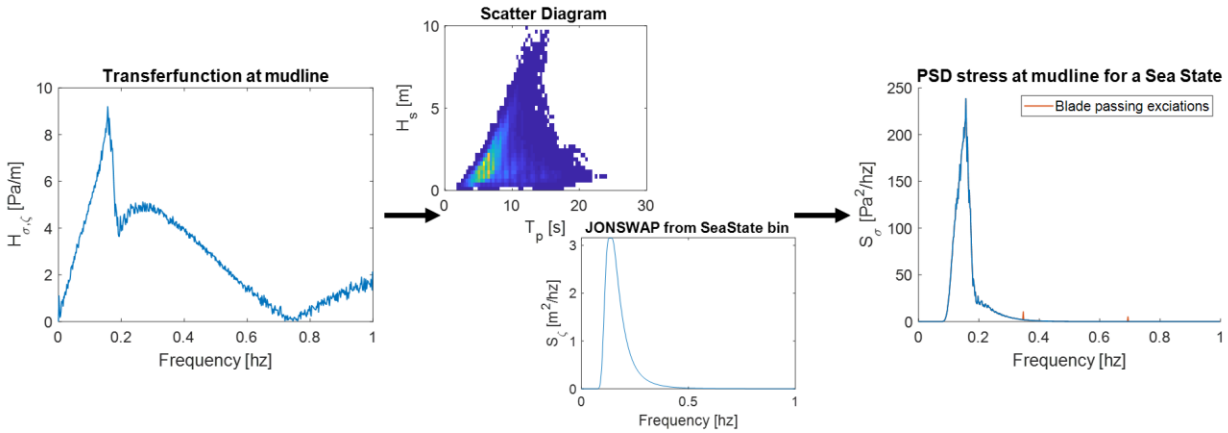

Figure 4-4: Overview of determining the stress spectrum $S_{\sigma,i,j}(f)$ for each $H_{s,i} - T_{p,j}$ class in the scatter diagram including the aerodynamic blade passing excitations

Here, m_i represents the i^{th} spectral moments. If $\beta \geq 0.96$ the stress spectrum is considered as narrow banded. Otherwise, the spectrum is wide banded. The moments are calculated by the numerical integration method, the trapezium rule.

For a narrow banded spectrum, the short term stress ranges follow a Rayleigh distribution. As the spectrum is assumed narrow banded, the equivalent stress ranges represent a constant amplitude stress. Assuming a single slope S-N curve, with component m the equivalent stress range is defined as.

$$\sigma_{eff} = \sqrt{8m_0}\left(\Gamma\left(\frac{2+m}{2}\right)\right)^{1/m}$$

Where, m_0 represents the zeroth spectral moment of the stress spectrum $S_{\sigma,i,j}(f)$ and $\Gamma(\cdot)$ is the gamma function. Using this relation, the short-term fatigue damage can be calculated as follows.

$$d(H_{s,i}, T_{p,j}, U_{w,k}, \theta_{wi,l}, \theta_{rel,m}, \phi) = T\sqrt{\frac{m_2}{m_0}}\frac{\sigma_{eff}^m}{A}$$

Where T represents the time (1 hour simulations), $\sqrt{m_2/m_0}$ represents the inverse zero crossing period term, and A, m the material fatigue parameter from the S-N curve along with the slope respectively. For this thesis, the material parameter of S-N curve 'D' in sea water under cathodic protections is used.

For a broad banded spectrum, numerous empirical solutions have been proposed by researchers. These include Wishing and Light's [82], Chaudhury and Dover's [83], Hancock and Gall's [84], and Dirlik's [85] empirical solution. Among these, Dirlik's empirical solution has been found to be most accurate with the approximations of rainflow counting. Therefore, Dirlik's empirical solution is used in this thesis.

Dirlik's empirical formulation is based on many numerical simulations using different spectral shapes. From these simulations Dirlik formulated an expression for rainflow ranges, $p_{RF}(\sigma_r)$, which is documented in the book Dynamics of Fixed Marine Structures [81] in equation 11.61.

Using Dirlik's empirical equation for the probability of rainflow ranges $p_{RF}(\sigma_r)$ the equation for short term damage in time T is as followed.

$$d(H_{s,i}, T_{p,j}, U_{w,k}, \theta_{wi,l}, \theta_{rel,m}, \phi) = \mathrm{T}\sqrt{\frac{m_4}{m_2}}\frac{1}{A}\int \sigma_r^m p_{RF}(\sigma_r)\, d\sigma_r$$

Here, $\sqrt{m_4/m_2}$ represents the inverse mean time in between peaks and A and m are parameters from the S-N curve.

Plotting the short-term fatigue damage $d(H_{s,i}, T_{p,j}, U_{w,k}, \theta_{wi,l}, \theta_{rel,m}, \phi)$ over the wave scatter diagram for a certain wind class $U_{w,k}$ and wind direction, $\theta_{wi,l}$, for aligned waves, $\theta_{rel,m}$, for a cross-sectional monopile node ϕ gives the following damage matrix.

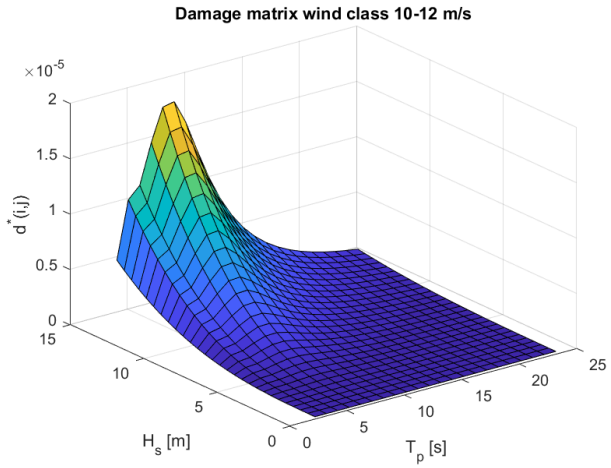

Figure 4-5: Example damage matrix for aligned wind class 10-12 m/s at mudline level

As the purpose of this research is in comparison of fatigue and not in building a confidence factor in design, no stress concentration factors, nor safety factors are included in the calculation.

4.2.3 Long term damage

For the long-term fatigue damage, the short-term fatigue damage is multiplied by the probability of occurrence and the design life, $T_{DL} = 25$ years, of the structure. Summing the damages per wind bin gives the following total damage on a monopile node at mudline.

$$D(\phi) = \sum_{k=0}^{U_{wcu}} \sum_{m=0}^{360} \sum_{l=0}^{360} \sum_{j=2}^{T_{p,max}} \sum_{i=0}^{H_{s,max}} T_{DL} \cdot P(H_{s,i}, T_{p,j}, U_{w,k}, \theta_{wi,l}, \theta_{rel,m}) \cdot d(H_{s,i}, T_{p,j}, U_{w,k}, \theta_{wi,l}, \theta_{rel,m}, \phi)$$

This equation considers all damages in operating wind conditions considering full directionality and wind-wave misalignment. Furthermore, ϕ, represents the cross-sectional node on the monopile, as shown in Figure 4-2.

4.2.4 Checks

Estimating fatigue in the frequency domain is sufficient as non-linear effects are normally not governing when conducting fatigue analysis. The reasoning is that fatigue is usually dominated by many small stress ranges for which the environmental loading and structural response are generally approximately linear. The spectral analysis procedure described above in section 4.2 is therefore satisfactory for fatigue

calculation. Nevertheless, care must be taken in linearising the load effect. Therefore, multiple checks have been performed.

The first check is conducted by analysing the computed stress spectra. The second check analyses the damages checking if the fatigue domain approach for OWT is valid. Thereafter, the effect of the MacCamy and Fuchs diffraction term implementation is touched on.

4.2.4.1 Stress spectrum

The methodology of deriving the stress spectrum according to section 4.2.1 is checked by comparing the stress power spectral density, $S_{\sigma,i,j}(f)$ derived according to Figure 4-4, to the stress response power spectral density derived using the according JONSWAP wave spectrum as input. Figure 4-6 provides a visualisation of this check.

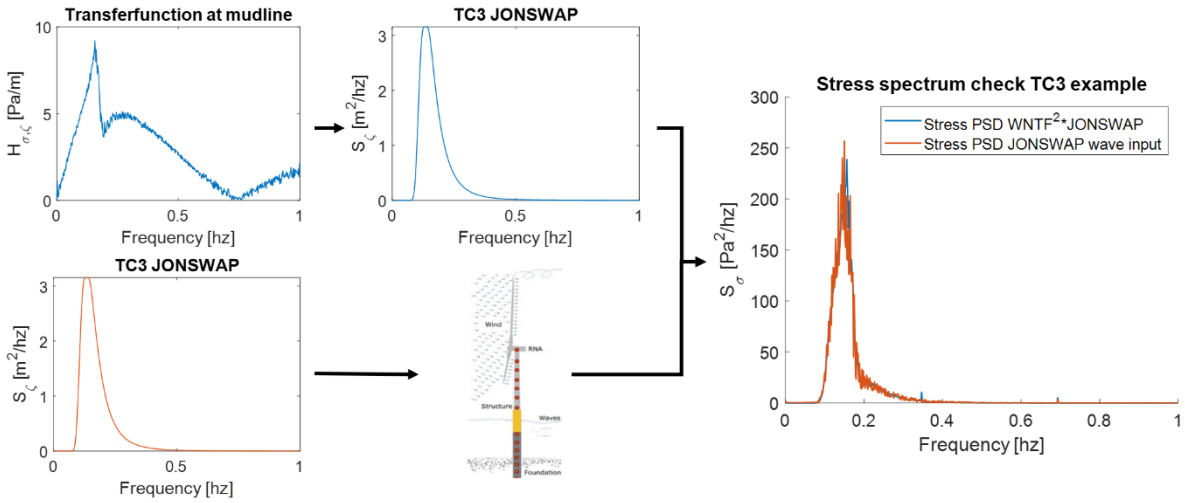

Figure 4-6: Visualization stress spectrum check example

The zeroth order moment of both spectra (m_0) are compared for different wind speeds and $H_s - T_p$ values. The results are shown in

Table 4-2. The differences are considered reasonable regarding fatigue estimations.

4.2.4.2 Damage

The unit fatigue frequency domain damage approach described in section 4.2.2 is checked by comparing the unit fatigue damage with full time domain unit fatigue damage results for 5 test cases. The full time domain damage approach uses S-N curve 'D' in cathodic conditions together with Palgrem-Miners linear damage hypothesis using rainflow counting, as section 2.2.3 concluded this is the most common practice.

Table 4-2 presents the results, showing differences in the range of 10% compared to the frequency domain approach used in this research.

The results show differences in the range of 10%. Based on the check by Katsikogiannis and the damage differences presented in

Table 4-2, it is concluded that Katsikogiannis' approach to determine long term fatigue damage has been correctly reproduced and incorporated in this thesis.

Table 4-2: Stress spectrum difference and damage difference of several test

Test Case aligned waves	Environment	Stress spectrum difference	Damage difference
TC1	H_s = 0.75 m; T_p= 4.5 s; U_w = 5 m/s	*3.4%*	*12.2%*
TC2	H_s = 1.25 m; T_p= 9.5 s; U_w = 9 m/s	*2.0%*	*11.6%*
TC3	H_s = 1.25 m; T_p= 7.5 s; U_w= 11 m/s	*1.1%*	*9.6%*
TC4	H_s = 4.75 m; T_p= 10.5 s; U_w= 15 m/s	*2.8%*	*10.3%*
TC5	H_s = 6.25 m; T_p= 12.5 s; U_w= 21 m/s	*0.1 %*	*8.9%*

4.2.4.3 MacCamy and Fuchs implementation

As mentioned in section 3.3.2 OpenFAST V3.5 does not include the MacCamy and Fuchs correction to incorporate diffraction. However, as mentioned in section 2.3.1 the diffraction effect for large monopiles has significant effect on the fatigue damage.

Diffraction is of relevance under the conditions, $D > 0.2\lambda$, meaning at wave lengths smaller than 50 meters for the waterline monopile dimensions, 10 meters, used for this thesis. Using the dispersion relation assuming deep waters, it can be concluded that diffraction is of relevance when considering for wave frequencies larger than 0.18 hz. Figure 4-7 shows that applying the MacCamy correction leads to a reduction of the spectral order moment of the transfer function for frequencies larger than 0.18 hz.

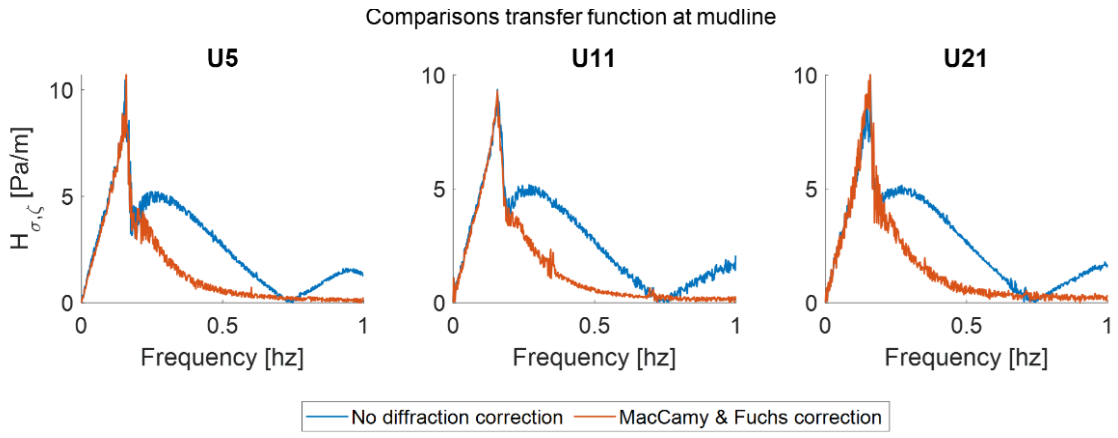

Figure 4-7: Comparison of transfer function visualizing the effect of diffraction in the spectrum for certain wind speeds

Section 4.2.2 shows that the spectral fatigue damage is dependent on the spectral order moments of the stress spectrum. Figure 4-7 shows the spectral order moment will decrease as the spectral order moment of the transfer function decreases, which will result in a decrease of the stress spectral order moment. Therefore, neglecting the MacCamy & Fuchs diffraction correction will overestimate the wave induced fatigue damage in this thesis.

4.3 MONOPILE GUYED LINE DIMENSIONS

Section 2.5 shows literature agreeing on mass reductions when implementing guyed lines to a monopile. To study the effects of adding guyed lines to a monopile, assumptions need to be made on how much steel can be saved compared to a conventional monopile design.

A significant decrease in monopile diameter is assumed. In addition, it is assumed the monopile diameter can not be smaller than the tower base diameter. Therefore, the minimum diameter throughout the length of the monopile is 10 meters for both the 15MW and 22MW turbines. Furthermore, the length of the guyed monopile remains the same as for the conventional monopile. The 15 MW monopile foundations for 40 meters water depth have been neglected as the base diameter for the conventional monopile is 10 meters. Therefore, no dimension reduction is possible using the methodology described above.

5 METOCEAN CONDITIONS

The previous section explains the methodology used to answer the research questions. In this section, the metocean analysis is discussed highlighting differences in geographical metocean conditions. These regional differences in metocean conditions show fatigue variations documented in section 6. This section is split in three sections. Section 5.1 documents the data which is used, section 5.2 shows the results of the analysis performed and section 5.3 concluded the findings of the analysis.

5.1 METOCEAN DATA

The metocean data is downloaded using a Shell license for the Metocean on Demand (MOOD) DHI portal. From this portal, wind and wave hourly hindcast data can be extracted from around the world. An overview of the locations and period of which the hourly hindcast data is extracted from is shown in Table 5-1. The three locations were selected because of their potential for future wind projects.

Table 5-1: Mood data collected from the MOOD DHI portal

	Baltic Sea	**East Coast US**	**North Sea Denmark**
Coordinates	55.851 Lat; 17.599 Long	41.579 Lat; -67.154 Long	55.477 Lat; 6.034 Long
Time period	1979-01-01 – 2023-01-10	1979-01-01 – 2023-01-07	1995-01-01 – 2018-31-12

5.2 METOCEAN ANALYSIS

Three different metocean analysis have been performed which are of relevance to fatigue:

- General metocean conditions
- The wave energy density spectrum
- Wind-wave misalignment

The results of these analysis have been documented below.

5.2.1 General metocean conditions

Figure 5-1 shows the scatter density plots of the main metocean parameters from the MOOD DHI hindcast data. The plots illustrate the joint distribution of the variables per location. Figure 5-2 presents the wind and wave roses, giving a graphical representation of the wind and wave directionality combined with the sea component.

In addition, an extremes analysis is performed using the Gumbel distribution. For offshore wind a 50-year extreme is typically used. Table 5-2 gives an overview of the 50-year extremes and mean of the three geographical regions considered.

Table 5-2: The 50 year extreme (P_{50}) and mean (μ) wave height and wind speed of the three regions considered

Values	**Baltic Sea**	**East Coast US**	**North Sea**
$\mathrm{P}_{50}\ H_s$ [m]	9.10	13.2	11.9
$\mathrm{P}_{50}\ U_w\ @10\ m$ [m]	42.4	53.6	51.4
$\mu\ H_s$ [m]	1.24	1.81	1.79
$\mu\ U_w\ @10\ m$ [m/s]	8.04	7.86	8.25

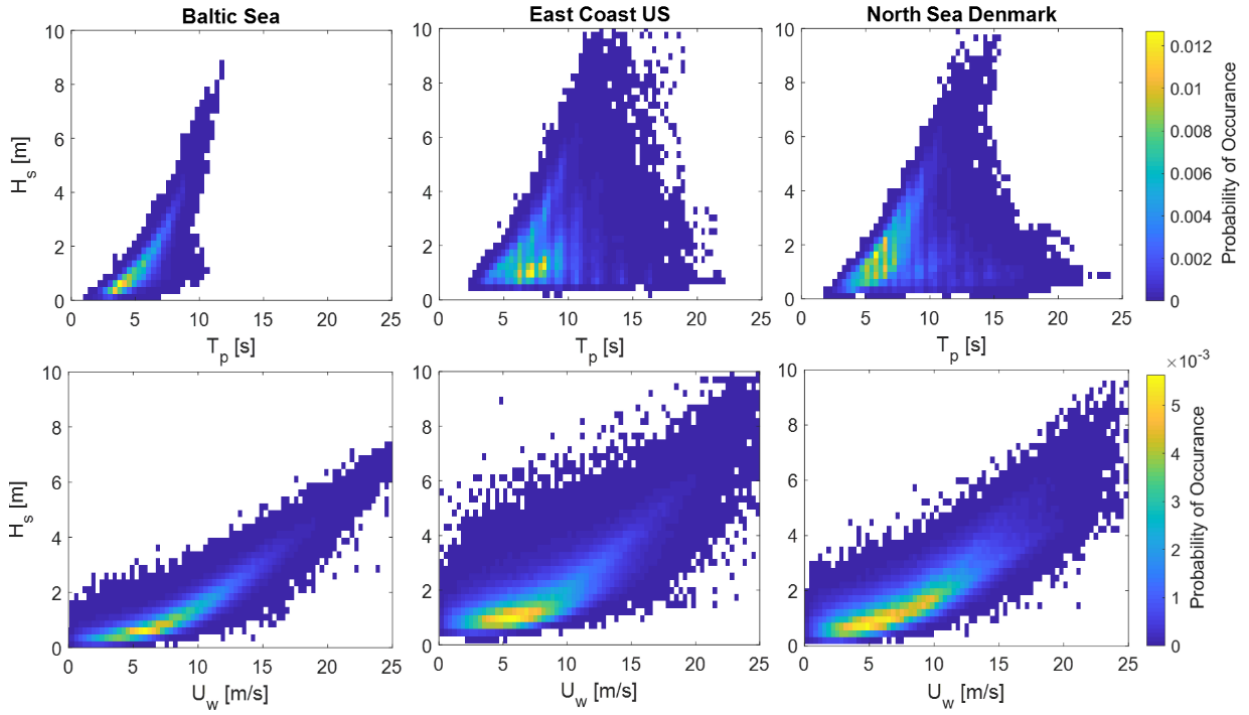

Figure 5-1: Scatter diagram of metocean conditions $T_p - H_s$ (top) and $U_w - H_s$ (bottom) at 10 m above MSL

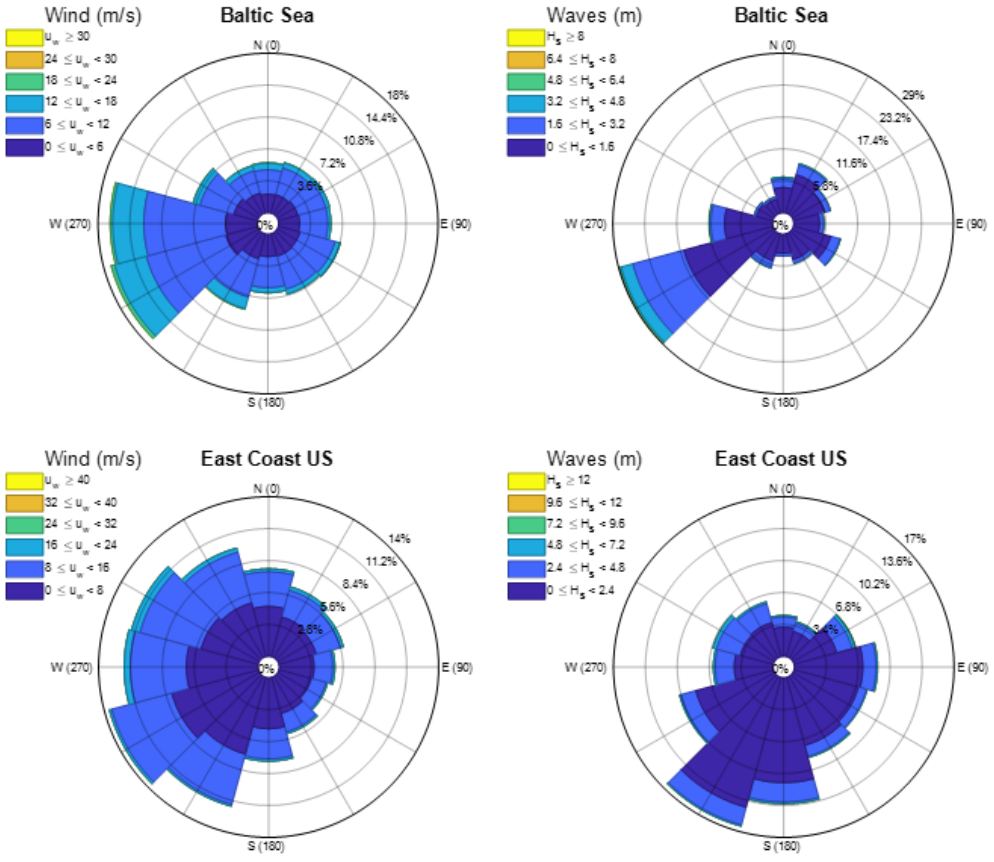

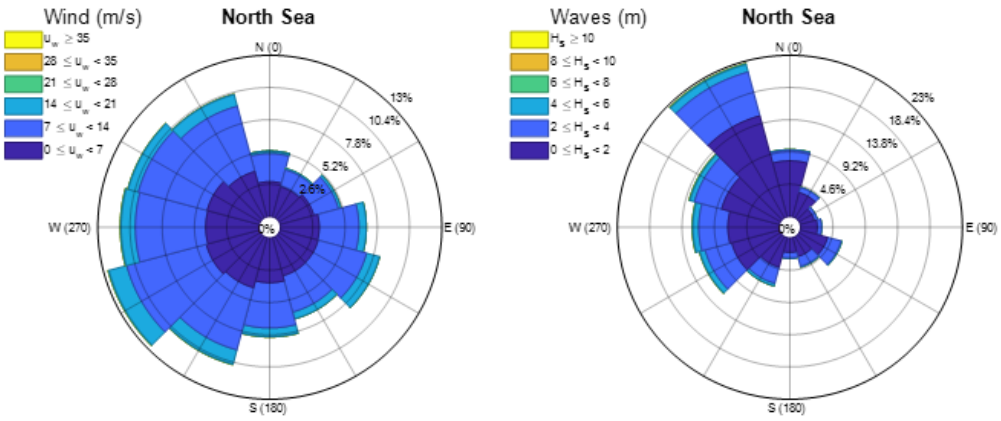

Figure 5-2: Wind and wave roses of the Baltic Sea, US East Coast and North Sea respectively

5.2.2 Wave energy density spectrum

Using the 1 hour time series data of significant wave height (H_s) and the mean wave period (T_{01}) the energy density spectrum is computed in accordance to Holthuijsen [86]. Figure 5-3 shows the energy density spectrum of the waves with respect to the natural frequencies of the turbine and conventional monopile considered in this thesis.

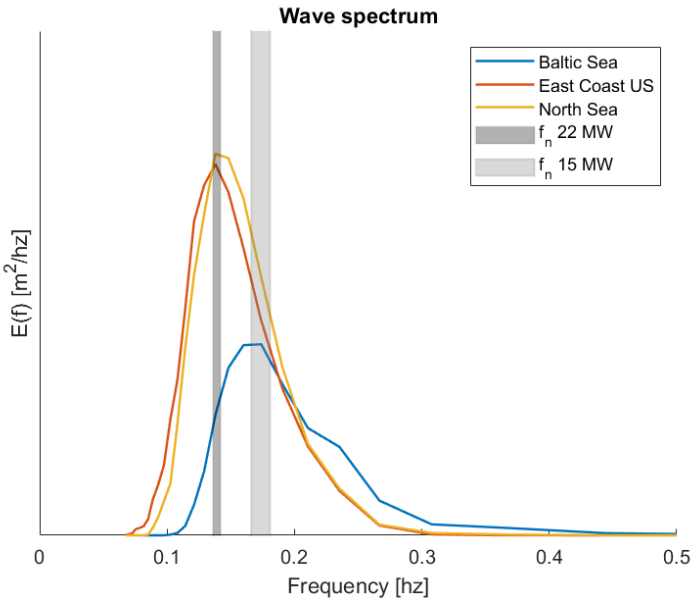

Figure 5-3: Energy density wave spectrum including the first natural frequency range of the 22MW turbines considered in this thesis

5.2.3 Wind-wave misalignment

Section 2.2.1 illustrated the importance of considering wind-wave misalignment in fatigue calculations as the aerodynamic damping is lower for these cases. Figure 5-4 shows the probability of occurrence of the wind wave misalignment bins over wind speed and the probability of the misalignment in total.

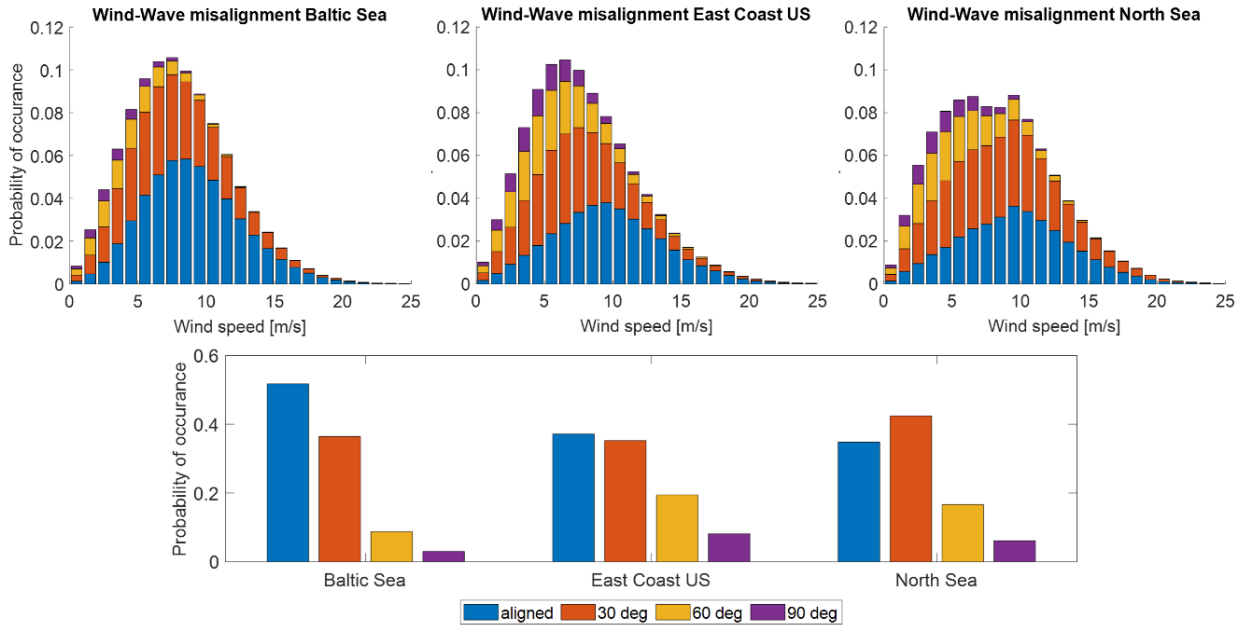

Figure 5-4: Wind-Wave misalignment with respect to wind speed (top) and the probability of the misalignment bin (bottom)

5.3 METOCEAN FINDINGS

The $T_p - H_s$ scatter diagram, Figure 5-1, shows distinct sea state characteristics across the different regions. In the Baltic Sea, the diagram indicates a wind sea state, whereas both the US East Coast and the North Sea show wind-swell sea state characteristics. The scatter diagrams further show that the Baltic Sea experiences shorter waves and smaller significant wave heights compared waves observed on the East Coast of the US and the North Sea, which is also concluded in the general analysis, Table 5-2.

The peak period, Figure 5-3, of these longer waves observed on the US East Coast and the North Sea align with the natural frequencies of the 22MW monopiles, documented in Table 3-3. This alignment suggests a potential for resonance in these regions. Conversely, the natural frequencies of the 22MW monopiles are outside the peak frequency in the Baltic Sea. Regarding the 15MW monopile natural frequencies documented in Table 3-2, the Baltic Sea peak wave frequencies show alignment. The $T_p - H_s$ scatter diagram also highlights a higher density of larger waves at peak periods between 6 and 8 seconds in the North Sea compared to the US east coast, which can also be seen in the wave energy density spectrum in Figure 5-3.

The $U_w - H_s$ scatter diagram, Figure 5-1, and wind-wave misalignment plots, Figure 5-4, show a similar distribution of wind probability densities for the Baltic Sea and the US East Coast, though with higher densities at larger significant wave heights for the latter. In contrast, the North Sea shows a higher density at higher wind speeds compared to the US East Cast and the Baltic Sea, along with a greater probability density of significant wave heights at these higher wind speeds.

The wind rose diagrams indicate a narrower directional spectrum for the Baltic Sea, in contrast to wider directional spectrums for both the US East Coast and the North Sea. The wave rose diagrams show a narrower directional spectrum for both the Baltic Sea and the North Sea, while the US East Coast shows a wider directional spectrum of waves.

The wind-wave misalignment distributions, Figure 5-4, reveal a Rayleigh distribution, with high probabilities of misaligned waves at low wind speeds, which gradually decrease with higher wind speeds. The Baltic Sea has the highest occurring percentage of aligned waves and exhibits the lowest probability density of misaligned waves larger than 30 degrees. The East Coast of the US and the North Sea both have equal probabilities of aligned waves. Compared to the US East Coast, the North Sea has higher probabilities of 30 degree misaligned waves, whereas the occurrences of misaligned waves larger than 30 degrees is lower.

Finally, the extremes analysis concludes that the highest extremes occur on the US East Coast, whereas this region experiences the lowest mean wind speeds and a comparable mean significant wave height with the North Sea.

6 FATIGUE OF THE CONVENTIONAL MONOPILE

The fatigue analysis results for conventional monopiles with detailed examinations of various parameters are considered in this section. Unless otherwise noted, the analysis incorporates the joint probability of metocean conditions as described in section 4.1, under operational wind conditions, hence for wind speeds between 3-25 m/s. In addition, a realistic percentage of idling over the lifetime in operational wind conditions is assumed. Therefore, idling for metocean conditions below cut-in and above cut-out wind speeds is not considered in this research. Furthermore, only the mudline cross-section of the monopile is analysed as this is identified as the weakest link in section 4. The cross-section has been divided into 72 nodes, where results in this section only document the maximum fatigue damage node along this cross-section.

The full results from the fatigue analysis are documented in appendix B. As visualised in these plots the fatigue damage is lower than 1, meaning the monopile will not fail due to fatigue according to the methodology used in this thesis research, which excludes safety factors and stress concentration factors. However, direct comparisons between results for different water depths and soil parameters are difficult, as the monopile designs are optimized for these parameters using the initial monopile design tool, section 3.2.

The monopile optimization ensures the stress and fatigue damage along the length of the monopile to be equal. As reported in section 4.2.1, stress is influenced by excitation forces and moments, and monopile dimensions. Therefore, the monopile dimension for each water depth and soil combination differs. To allow for sensible comparisons and to identify trends between the geographical areas, the results have been normalized for each water depth and soil parameter combination.

Section 6.1 shows the effect of wind-wave misalignment, section 6.2 shows how idling affects the fatigue damage, whereafter 6.3 combines these effects and compares the geographical regions. Finally, section 6.4 shows how the size of the turbine influences the fatigue damage. This section is concluded with a general discussion.

6.1 WIND-WAVE MISALIGNMENT

This section provides an analysis of the effect of wind-wave misalignment on monopile fatigue damages when only considering the turbine in operational conditions. The differences in fatigue damage considering solely aligned waves and including wind-wave misalignments are visualized in Figure 6-1. The hue colour assumes the metocean conditions to be fully aligned throughout the 25 year lifetime, by scaling these probabilities of occurrences from the metocean analysis in section 5 accordingly. The tinted colour shows the total fatigue damage when incorporating the misalignment in accordance with sections 1-1. The results have been normalised to the sum of the fatigue damage for each monopile specific design condition.

Figure 6-1 shows that when considering only aligned waves, the total fatigue damage in the Baltic Sea is the lowest. As concluded in section 5.2.2, the Baltic Sea experiences the lowest energy density of waves leading to a reduced fatigue damage for all monopile design conditions, considering the three geographical regions. Even when considering that both wind and waves have a narrow directional

spectrum. Hence, it is concluded that that the energy density of waves at the natural frequency has higher influence on fatigue damage than the wave directional spreading.

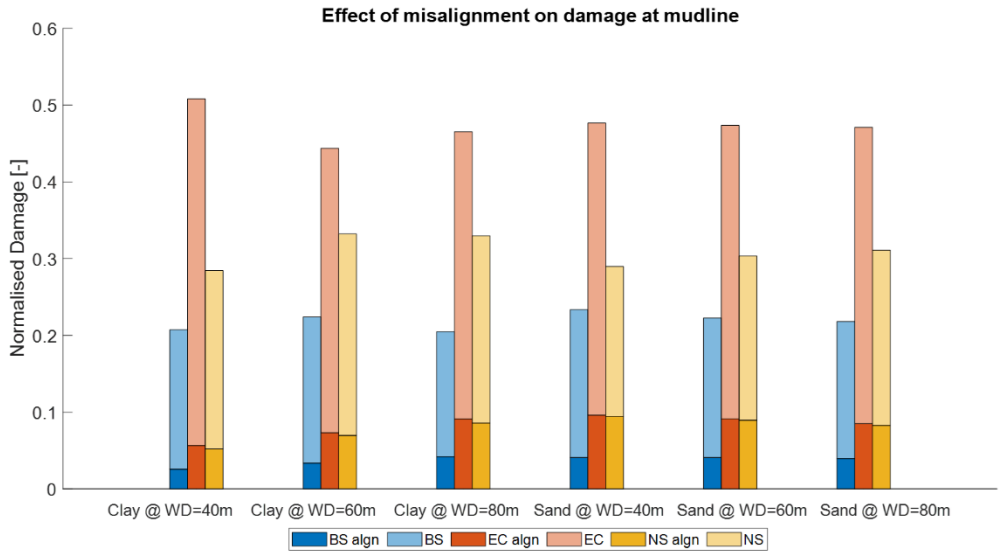

Figure 6-1: Normalized wind-wave misalignment fatigue results at mudline compared to fully aligned wind-wave conditions for all regions, water depths and soil parameters regarding the 22MW turbine

Furthermore, Figure 6-1 shows that when considering only aligned waves, the total fatigue damage of the North Sea and the US East Coast is similar. As concluded in section 5.2.2 both locations have comparable wave energy spectra, with the North Sea having slightly more energy compared to the East Coast. Section 5.2.1 concluded a narrow wave direction spectrum in the North Sea, whereas the East Coast experiences a wider wave direction spectrum. Both regions have a wide wind direction spectrum, which will typically result in higher fatigue damages for the North Sea. However, the US East Coast experiences slightly lower wind speeds, as concluded in section 5.2.3, leading to reduced aerodynamic damping as discussed in section 2.2.1. Consequently, when only considering wind-wave alignment the highest fatigue damage for 22 MW turbine monopile foundations occurs in the US East Coast.

Considering misaligned waves Figure 6-1 illustrates larger differences in fatigue damage. Section 5.2.3 notes that the US East Coast has a higher probability of extreme misalignment, larger than 30 degrees, compared to the North Sea whilst having similar probabilities of aligned waves. These cases benefit less from aerodynamic damping, resulting in larger differences in fatigue damage for misaligned waves than when only considering aligned waves.

Hence, including misalignment increases the fatigue damage. This is aligned with the conclusions from Santos et al. [34] and Horn et al. [35] as documented in section 2.2.1. Horn et al. [35] showed that including wind-wave misalignment contributes to 30% of the fatigue damage on a 9 meter diameter monopile. In this research the fatigue damage contribution on a 10 meter diameter monopile ranges between 200%, for the Baltic Sea and 400% for the East Coast. Conclusions from Velarde et al. [11] and Santos et al. [34], both identifying higher hydrodynamic fatigue contributions for larger monopile diameters, partially explain this difference. However, the largest contribution to this difference, originates from the uniform wind assumption in this research.

Turbulent wind results in a fluctuating thrust force at hub height over time, compared to a steady thrust force when assuming uniform wind conditions. The fluctuating thrust force causes a larger bending moment amplitude magnitude at mudline resulting in higher fatigue damages on the monopile nodes in the FA direction. This is visualized in Figure 6-2 to Figure 6-4 where the damage roses over the mudline monopile cross-section are shown. In these figures the wind comes from the north (0 degrees) and the wave directions vary (0, 30, 60, 90 degrees) according to the title. For these plots a standard turbulence intensity (IEC 14.4) is used.

The figures show significant differences in fatigue damage over the mudline cross section of the monopile when considering turbulent winds. Evaluating the maximum damage, it can be concluded that for full-aligned waves the maximum fatigue damage significantly differs. For low wind speeds, Figure 6-2, the maximum fatigue damage assuming uniform wind conditions is a factor 10 lower than when considering turbulent wind. For higher wind speeds, Figure 6-4, the difference decreases to a factor 3, as high wind speeds produce higher waves, leading to larger bending moments caused by hydrodynamics. Regarding fully-misaligned waves, the maximum fatigue damage magnitude assuming uniform wind conditions correlate with the fatigue damages using turbulent winds. Minor differences in maximum fatigue damage on the location of the cross-sectional node are seen for low fully-misaligned wind speeds, Figure 6-2. This is caused by low aerodynamic damping for low wind speeds cases due to low rotational rotor speeds. Furthermore, the fatigue damages roses also indicate that for smaller misalignment angles, the differences in damage assuming uniform wind or turbulent wind conditions are larger, especially at lower wind speeds.

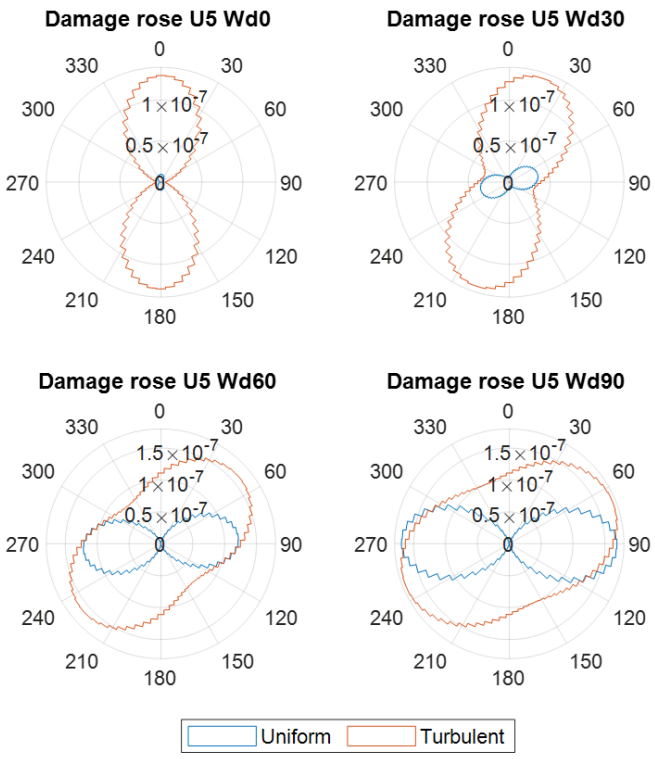

Figure 6-2: Wind-Wave misalignment cases damage rose for low wind speeds with wind always coming from the north

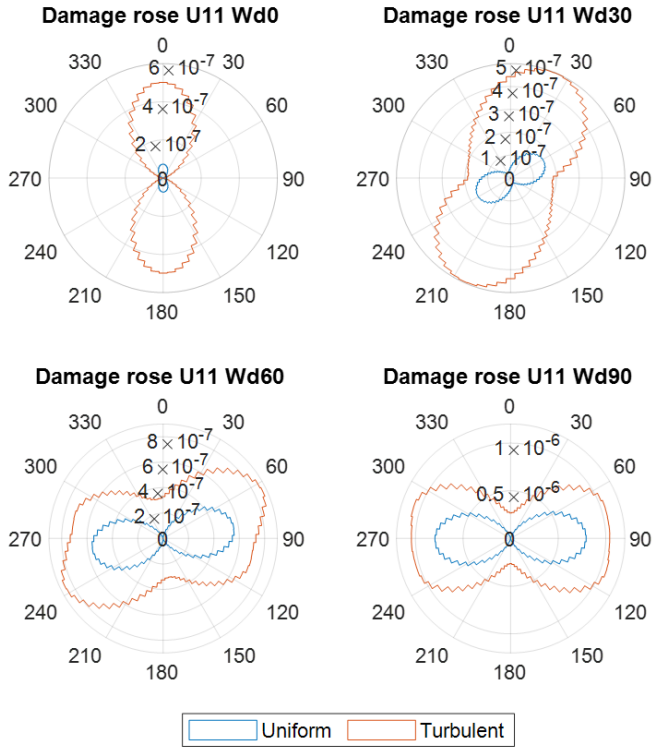

Figure 6-3: Wind-Wave misalignment cases damage rose for rated wind speeds with wind always coming from the north

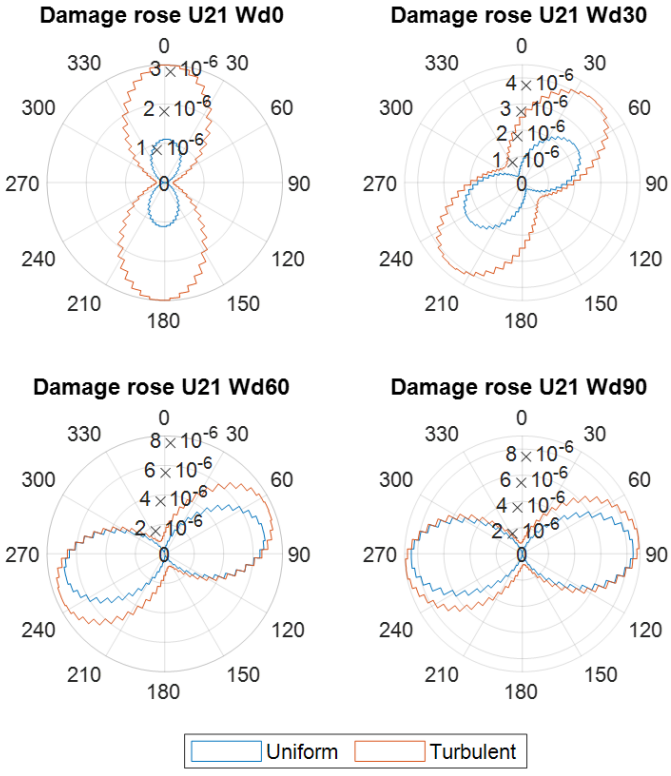

Figure 6-4: Wind-Wave misalignment cases damage rose for high wind speeds with wind always coming from the north

However, both wind condition assumptions show an increase in fatigue damage magnitude with an increasing misalignment angle. Therefore, using uniform wind provides reasonable results to identify differences in geographical areas based on metocean conditions. However, the overall difference in fatigue damage for aligned and misaligned cases will be lower when considering turbulent wind, indicating that the fatigue magnitudes in Figure 6-1 will be less pronounced for all regions.

6.2 IDLING

The impact of an idling turbine on fatigue damage is elaborated on in this section. The cross-sectional node location of the maximum damage during idling is in line with the dominant wave direction. This node does not correlate with the location where the maximum fatigue occurs during operational conditions, as indicated in section 6.1.

The results, visualised in Figure 6-5, illustrate the effect of the assumed percentage of idling, during operational wind conditions, on the total fatigue damage. The mudline cross-sectional node with the largest fatigue damage over lifetime is documented. This node is not in line with the dominant wave direction. Additionally, the figure displays fatigue damage normalized to the maximum fatigue damage per pile, highlighting the effect of idling for all parameters.

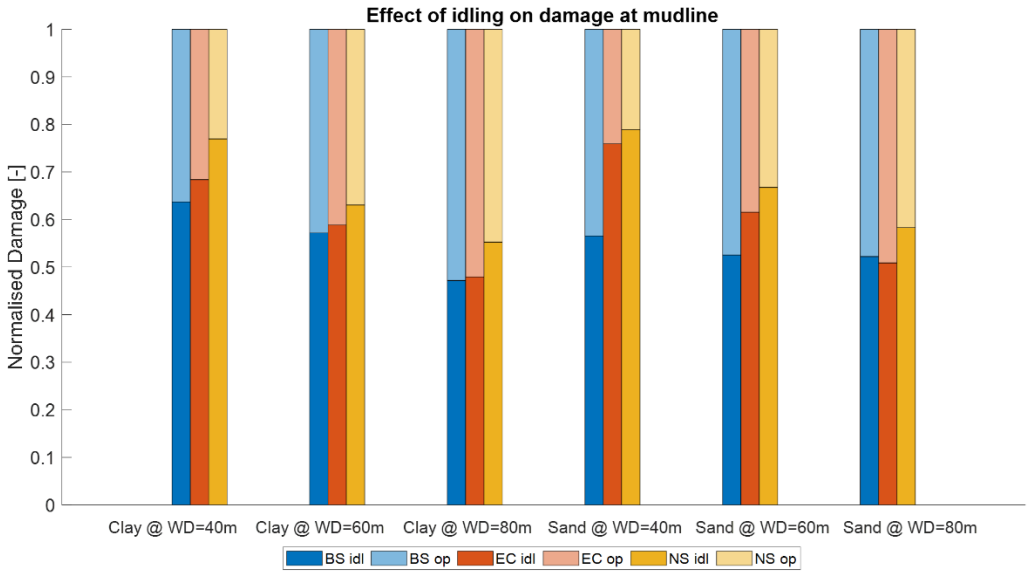

Figure 6-5: Operational and Idling normalized fatigue results for all regions, water depths and soil parameters regarding the 22MW turbine where 1 shows the total fatigue damage during operational wind conditions

Figure 6-5 shows that idling in the North Sea contributes the most to total fatigue damage across all water depths and soil profiles. This is due to the alignment of the natural frequency and the peak wave frequency as indicated in section 5.2.2 and the narrow directional spectrum of the waves compared to the wider directional wave spectrum on the US East Coast. In contrast, the Baltic Sea shows the lowest contribution of idling fatigue to the total fatigue damage because of the lower wave energy density. Therefore, it is concluded that, in the Baltic Sea, the wave contribution to the total fatigue damage is lower when compared to the other two regions.

The contribution of idling is higher in sand profiles for both the East Coast and the North Sea, caused by the differences in natural frequencies for the same water depths. As shown in Table 3-3, the natural frequency in clay profiles is lower than in sand profiles for the same water depths. At these lower frequencies the waves contain less energy, as visualised in Figure 5-3.

Additionally, water depth influences the effect of fatigue damage over the lifetime of the monopile foundations. At a water depth of 40 meters, the assumed percentage of idling period over the operational lifetime contributes to an average of 70% fatigue life damage. In contrast, at 80 meters depth, idling has a 50% contribution to fatigue life damage. The natural frequencies slightly influence these differences, however the largest contribution to these differences is caused by a form of hydrodynamic damping. As elaborated on in section 3.3.2, OpenFAST uses Morison's equation to model the hydrodynamic excitations. The equation relies on the relative velocity and acceleration between wave and structure for drag and inertia forces respectively. While wave velocities and accelerations remain constant, as wave inputs per water depth are assumed constant, the velocities and accelerations of the structure at water line level increases with deeper waters. Consequently, the hydrodynamic force acting on the structure decreases, providing a form of hydrodynamic damping.

6.3 Geographical regions

Combining the misalignment effects elaborated on in section 6.1 with the idling effect in section 6.2 illustrates the total fatigue damage and differences per geographical region. The results are visualised in Figure 6-6, where the total damage is normalised per monopile design based on soil profile and water depth.

For all water depths and soil conditions, it is concluded that the East Coast of the US consistently experiences the highest damage followed by the North Sea. Although these regions have similar wave energy density spectra, the East Coast of the US has less benefits from aerodynamic damping as a result of lower wind speeds and higher wind-wave misalignment probabilities concluded in section 6.1. In contrast, due to its lower wave energy density and highest wind-wave alignment probability, the Baltic Sea has the lowest damage.

Figure 6-6 reveals smaller differences in fatigue damage between the North Sea and the US East Coast compared to the operation conditions shown in Figure 6-1. The idling effect is most pronounced in the North Sea, significantly contributing to the overall fatigue damage.

When evaluating the North Sea and the East Coast of the US, it is concluded that wind-wave misalignment has a greater influence than wind-wave directionality over the lifetime of the monopile. Specifically, the narrow directional spectrum of waves in the North Sea, which are slightly more aligned, result in lower maximum fatigue damages, compared to the wider directional spectrum of waves with higher misalignment probabilities on the East Coast of the US. This conclusion is valid when assuming uniform wind conditions. However, when turbulent wind is considered, the effect may vary. As discussed in section 6.1, damages at a 30-degree misalignment angle will be higher.

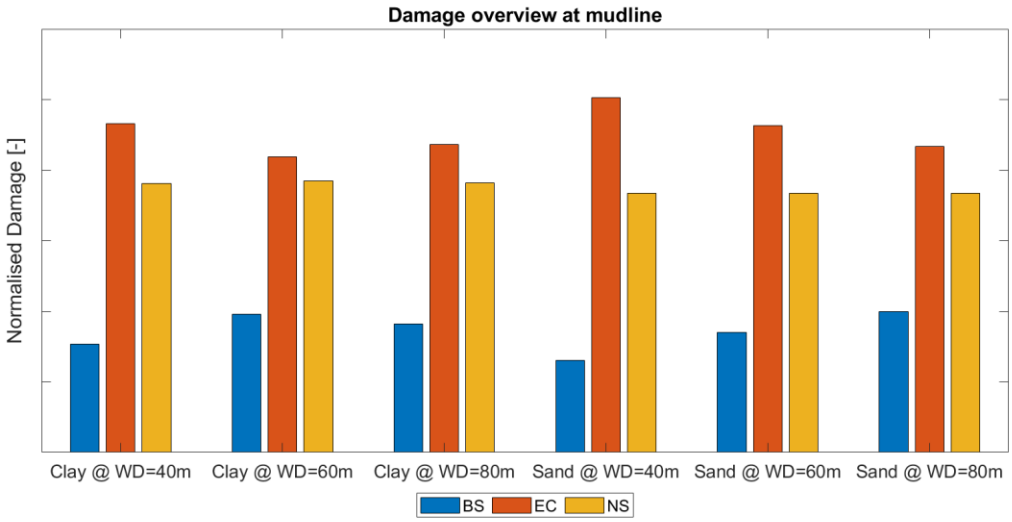

Figure 6-6: Normalized fatigue results for all water depths and soil parameters visualizing the differences between geographical regions regarding the 22MW turbine

6.4 Turbine size

The sections above illustrate the effects of wind-wave misalignment and idling on the fatigue damage of a 22MW monopile foundation across multiple water depths and soil conditions. This section shows the relation of turbine size on fatigue damage with respect to misalignment, Figure 6-7 and idling, Figure 6-8 effects. The same assumptions made in sections 6.1 and 6.2 also apply for this section. Furthermore, for clarity reasons, Figure 6-7 and Figure 6-8 plot solely the fatigue damages regarding sand profiles for all water depths and geographical regions to compare the fatigue damage results of 15MW and 22MW monopile foundations. The full results of wind-wave misalignment effects, idling effects and total fatigue damage are documented in appendix C.

Regarding misalignment effects, Figure 6-7 shows a wind-wave misalignment fatigue damage contribution for the smaller turbine ranging between 150% to 300%. This effect is less pronounced compared to the 22MW wind-wave misalignment fatigue damage contribution between 200% to 400%. Additionally, Figure 6-8 shows that idling contribution has less influence on fatigue damage for smaller turbines ranging from 60%-40% dependant on water depth, compared to the 70%-50% contribution concluded in section 6.2.

Both Figure 6-7 and Figure 6-8 conclude that the fatigue damage of 15MW turbine is less hydrodynamic dominant, which is caused by two effects. Firstly, the overall hydrodynamic excitation area of the monopile is less as the diameter of the monopile over the length is smaller. However, as the water line diameter of both the 22MW turbine monopiles and 15MW turbine monopiles is 10 meters this effect is not the largest. Secondly, the natural frequency of the monopile is shifted to higher frequencies, visualized in Figure 5-3. The figure shows that the natural frequency of the 15MW monopiles is shifted outside the peak energy spectrum of both the US East coast and the North Sea and the positioned right in the peak wave frequency of the Baltic Sea. Figure 6-8 clearly shows the consequence of this as the idling fatigue damage contribution has increased and become the highest for the Baltic Sea, whereas in both in the US East coast and the North Sea the contribution has decreased.

Therefore, it is concluded that regarding smaller turbines the wave contribution to fatigue damage is less for both the US East Coast and the North Sea and higher for the Baltic Sea. This is mainly caused by the placement of the natural frequency in the wave energy spectrum.

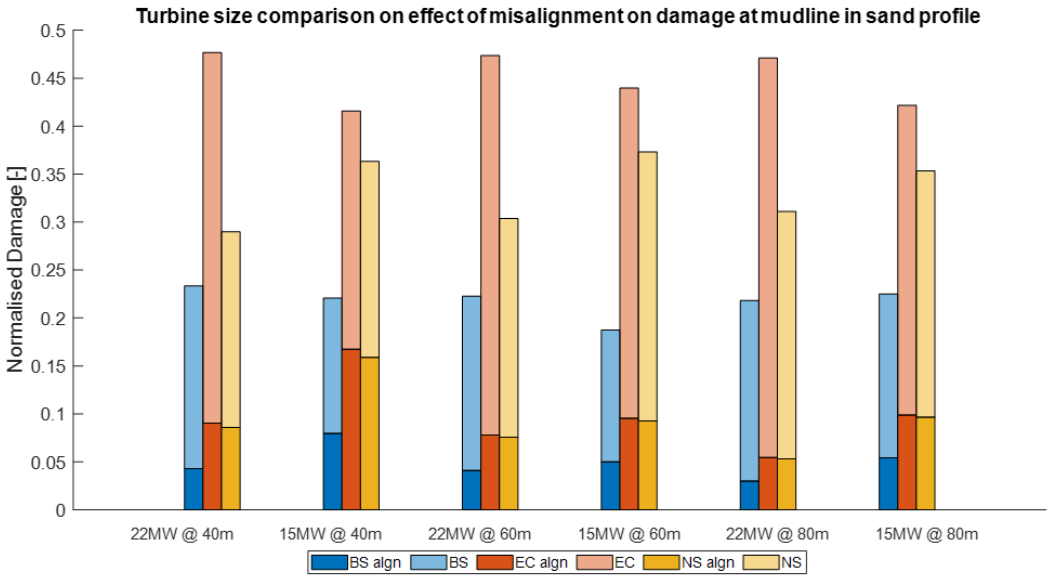

Figure 6-7: Normalized wind-wave misalignment fatigue results regarding 22MW and 15MW turbine at mudline compared to fully aligned wind-wave conditions for all regions water depths in sand profile

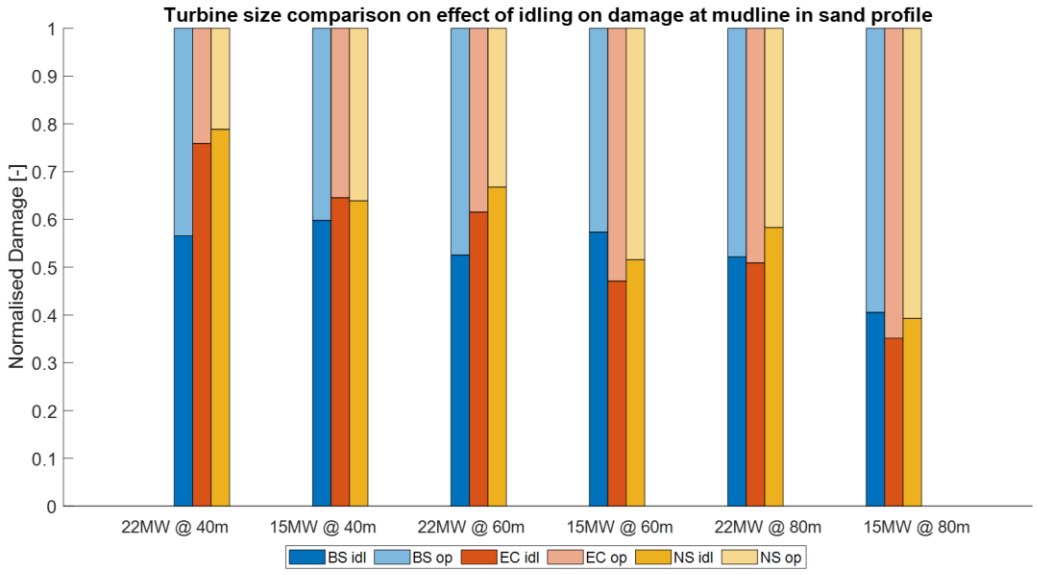

Figure 6-8: Operational and Idling normalized fatigue results regarding 22MW and 15MW turbines, for all regions, water depths in sand soil profile where 1 shows the total fatigue damage during operational wind conditions

6.5 General discussion

This section elaborates on the general assumptions made in the methodology and analysis of conventional monopile fatigue damage results, which influence the conclusions drawn.

The simulations were conducted using a representation of a white noise wave spectrum over a 1 hour period, assuming stationary environmental conditions. Since the natural frequency of the monopile is close to the peak energy spectrum, resonance can occur. However, this short representation of white noise potentially underestimates the amplitude of the stress response, resulting in an underestimation of the fatigue damage. This aspect is not further investigated in this thesis.

Furthermore, as elaborated on in section 6.1, the neglect of turbulence in the wind significantly underestimates the fatigue damage for aligned wind-wave conditions.

Additionally, literature, summarised in section 2.2.1, showed that soil damping is the second highest source of damping, following the dominant aerodynamic damping. Section 2.2.2 also concluded that the critical location regarding fatigue is slightly below mudline. However, due to limitations in OpenFAST V3.5.0, the numerical model does not include soil-structure interactions. Consequently, the results in this thesis do not include soil damping, which will have a positive effect of the fatigue damage. Moreover, this thesis neglects the reaction forces below mudline, which when included will potentially have a negative effect on the fatigue damage. Only structural damping, and structural stiffness have been included in the model.

Finally, the analysis does not take into account the effect of diffraction for large monopiles. Section 4.2.4.3 concluded that diffraction effects reduce the stress at wave frequencies larger than 0.18 hz. Disregarding this phenomenon results in an overestimation of fatigue damage. This means that for shorter wave periods, which mostly occur in the Baltic Sea, the fatigue damage has been over estimated. Therefore, the differences between fatigue damages in the Baltic Sea compared to the US East Coast and North Sea will likely be larger.

Despite these limitations, the primary goal of these results is to analyse regional differences in fatigue damage. Therefore, the conclusions drawn can still be considered valid.

7 GUYED MONOPILE SYSTEM

This section analyses the effect of the monopile guyed line system. Section 7.1 shows the results of the weight reduction strategy used in this thesis. Section 7.2 shows the relation between the stiffness of the tendon and the natural frequency of the whole system. For the fatigue results of the conventional monopile in section 6 the mudline was considered, however adding the tendons to the system changes the structural behaviour. Therefore, 7.3 discusses the critical location used for the fatigue analysis of the guyed monopile system. Section 7.4 compares the fatigue damage of the guyed line system to the conventional monopile. Finally, checks regarding snap loads risks of the tendons and an ULS check have been performed in section 7.5.

7.1 MP MASS REDUCTION

Table 3-2 and Table 3-3 show masses of the convention monopiles used for the fatigue analysis in section 6, up to 6,500 tons in 80 meter deep clay soil conditions. This mass results in high material costs and limits the availability of suitable installation vessels, thereby increasing the total costs.

Section 2.5 provides literature, that shows the guyed lines transfer a significant part of the wind and wave loads directly into the soil. Hence, reducing the stresses in the monopile. As a result, the monopile can be designed with smaller diameters and wall thicknesses.

As explained in section 4.3, the aim of this research is to demonstrate that the dimensions of the monopile can be reduced significantly when adding a guyed line system to the monopile. This reduction in mass not only lowers material costs but also expands the range of installation vessels.

The foundations for depths of 40 meters do not show mass reduction as the bottom diameter of the conventional monopile was 10 meters. Assuming the bottom diameter can not be smaller than the tower base diameter, 10 meters, no diameter reduction for the guyed monopile can be implemented, resulting in no mass reduction. Hence, the 15MW guyed monopile system in 40 meter water depths is not further analysed in this research.

The results show that, for 15MW turbines, the mass reduction is more significant for monopiles at 80 meters depth compared to those at 60 meters depth. The results demonstrate that at water depths deeper than 60 meters, the reduced mass percentage stabilizes for the guyed monopile foundations of the 22MW turbines.

This mass reduction increases the range of suitable installation vessels, as most vessels have crane hook safe working load (SWL) capacities of 3,000 tons. Only large oil and gas installation vessels can handle monopile masses exceeding 4,000 tons. Consequently, it is concluded that most of the modelled guyed monopiles, can be installed by a wider array of installation vessels compared to the conventional monopile in the same water depth.

This thesis does not analyse the potential decrease in embedment length, which could also be advantageous for guyed monopile systems.

7.2 TENDON LINE STIFFNESS

Reducing the diameter and wall thickness, as described in section 4.3, makes the OWT structure more compliant. Adding tendons ensures the systems stiffness, which can be adjusted by using stiffer lines. Thus, the stiffness of the guyed monopile system is directly correlated to the stiffness of the tendons.

The stiffness depends on the pretension and material selection defined by the product EA, where E is the modulus of elasticity and A is the area of the tendon line. The material selection is crucial in determining the tendon stiffness.

Furthermore, the stiffness of the guyed monopile is influenced by the configuration of the guyed system. As mentioned in section 3.4, this research considers tendons that are connected 10 meters below MSL at a 45-degree angle relative to the monopile.

Figure 7-1 illustrates the correlation between the tendon stiffness and the natural frequency of the guyed monopile system. For clarity reasons, the amount of parameters in Figure 7-1 is reduced to guyed monopiles in clay parameters. However, all conclusions below also apply to all other parameters.

Firstly, Figure 7-1 (top left) shows that the guyed monopiles in clay conditions are more sensitive to tendon stiffness than those in other soil conditions. Furthermore, as the water depth increases, the natural frequency of the system becomes more sensitive to tendon stiffness, visualized in Figure 7-1 (top right). In addition, Figure 7-1 (bottom left) reveals a larger natural frequency envelope when tendons are connected at MSL compared to 10 meters below MSL. For the configuration where tendons are connected at 10 meters below MSL, a 30 degree connection angle with respect to the monopile results in the largest natural frequency envelope. This setup requires the shortest tendon length, making it advantageous for tuning the systems natural frequency out of the wave spectrum. However, it also requires a large diameter tendon to match the conventional monopiles natural frequency. Finally, Figure 7-1 (bottom right) shows that for larger turbines, the envelope of the natural frequency is larger, resulting in a higher ability to tune the frequency.

Figure 7-1 show a theoretical relationship between natural frequency and tendon stiffness, however in reality, the high tendon stiffness is unfeasible to fabricate. For the stiffest available material on the mooring line market, Dyneema SK99, tendon diameters larger than one meter are required for stiffness greater than 1000 MN/m.

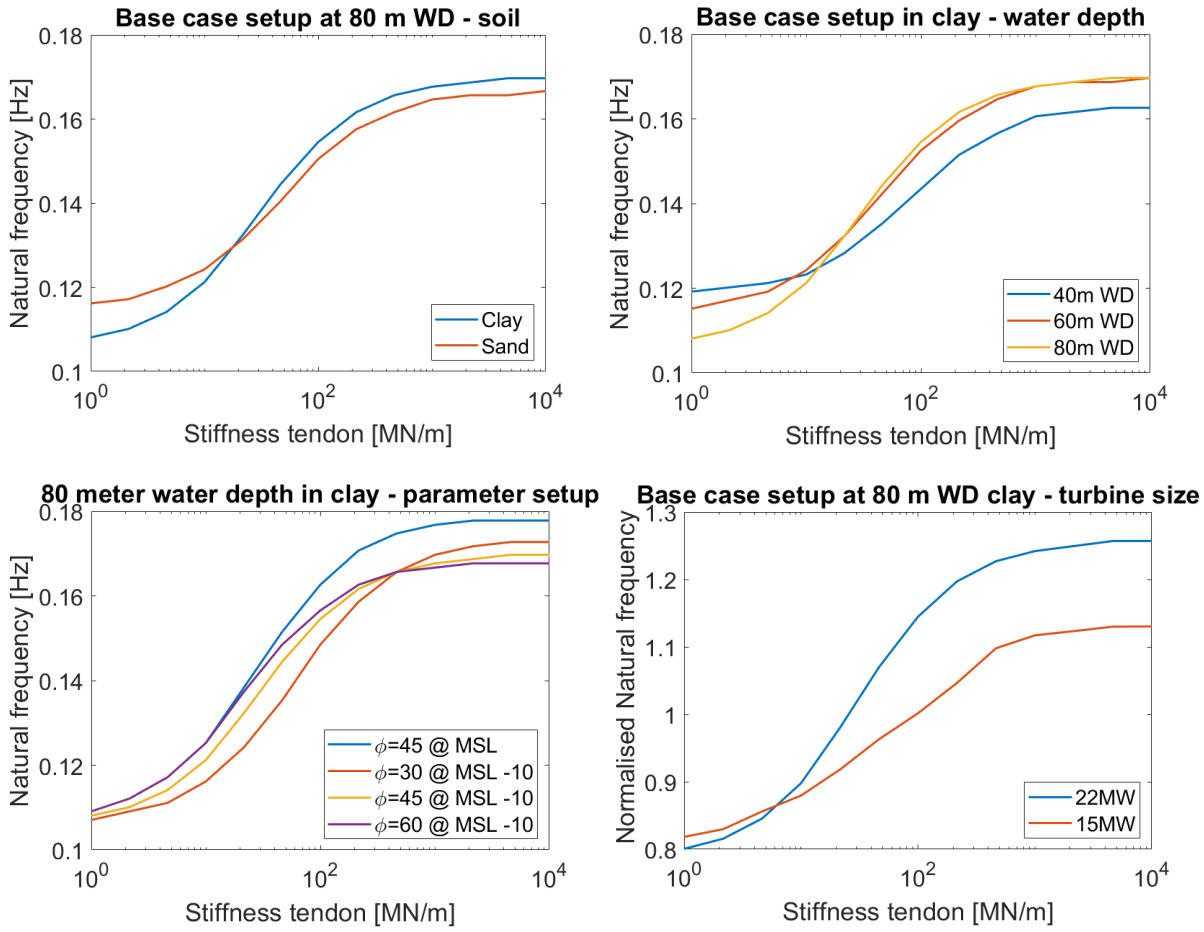

Figure 7-1: Tendon stiffness- f_n soil (top left), water depth (top right), parameter (bottom left) and turbine size (bottom right) comparison

7.3 CRITICAL LOCATION FOR FATIGUE ASSESSMENT

The monopile guyed system alters the system's structural properties. Figure 7-2 illustrates the change in moment line when the tendons are attached. This plot shows a representative change in moment lines for a 22MW monopile in 80-meter sand profile conditions for a given tendon stiffness, a trend consistent for all parameters analyzed in this thesis. The tendons used in this plot demonstrate a reduction in the mean moment magnitude after the tendon connection node. This indicates that the maximum mean moment magnitude occurs at the connection point. For stiffer tendons, the moment at the mudline is smaller than plotted below.

As elaborated in section 4, the weakest link analyzed for fatigue damage in this thesis is at the mudline. Figure 7-2 shows that for a conventional monopile model used in this research, the moment is largest at 80 meter water depth, which is at the mudline for this figure. Therefore, in the analysis of the guyed monopile system, the location with the largest mean moment magnitude is considered to be the weakest link. It is assumed that the largest mean moment also corresponds to the largest stress amplitudes at this location. Consequently, the critical point along the length of the monopile analyzed in this research is at the tendon connection node for the guyed monopile system.

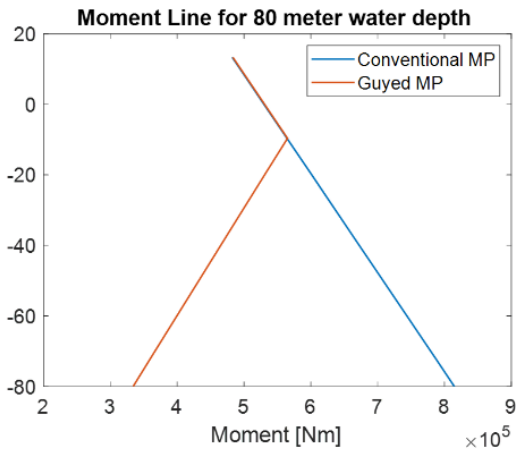

Figure 7-2: Example moment lines achieved by exciting an operational turbine to rated wind speeds

7.4 Fatigue

This section estimates the effect of guyed monopiles on fatigue damage compared to conventional monopiles as analyzed in section 1. The same methodology and assumptions that are used for the conventional monopile analysis are applied here. Therefore, the same discussion points apply as documented in section 6.5.

For the fatigue analysis of guyed monopiles, the base case setup is employed, with tendons connected at 10 meters below MSL at a 45-degree angle with the monopile. Regarding this setup, three assessments have been performed. First, the effect of tendon stiffness to fatigue damage has been documented in section 7.4.1. Second, a fatigue analysis at two separate locations along the monopile has been performed in section 7.4.2. Third, in section 7.4.3 the analysis is performed on the 15MW turbine, visualizing the differences in fatigue damage between the 15MW and 22MW turbine. All results have been normalized to the conventional monopile fatigue damage for the US East Coast under each monopile specific design condition.

7.4.1 Tendon stiffness correlation with fatigue

For this analysis, two tendon stiffness levels are analyzed and the results are shown in Figure 7-3. The 'GL (F)' configuration, meaning Guyed Line (Flexible), represents the fatigue damage results for tendon stiffnesses, aligning the natural frequency of the guyed monopile with the conventional monopile. The tendon stiffness values used originate from the results visualized in Figure 7-1 and are considered feasible as concluded in section 7.2. The 'GL (S)', configuration, meaning Guyed Line (Stiff), represents the fatigue damage of ultra stiff tendons. Although these tendons are unfeasible in practice, they illustrate the theoretical potential of the guyed line system with respect to fatigue reduction.

All three configurations show fatigue results at the critical locations that are identified in this thesis. For the guyed monopile system, the tendon connection node is analysed, while for the conventional monopile, the mudline fatigue damage is examined.

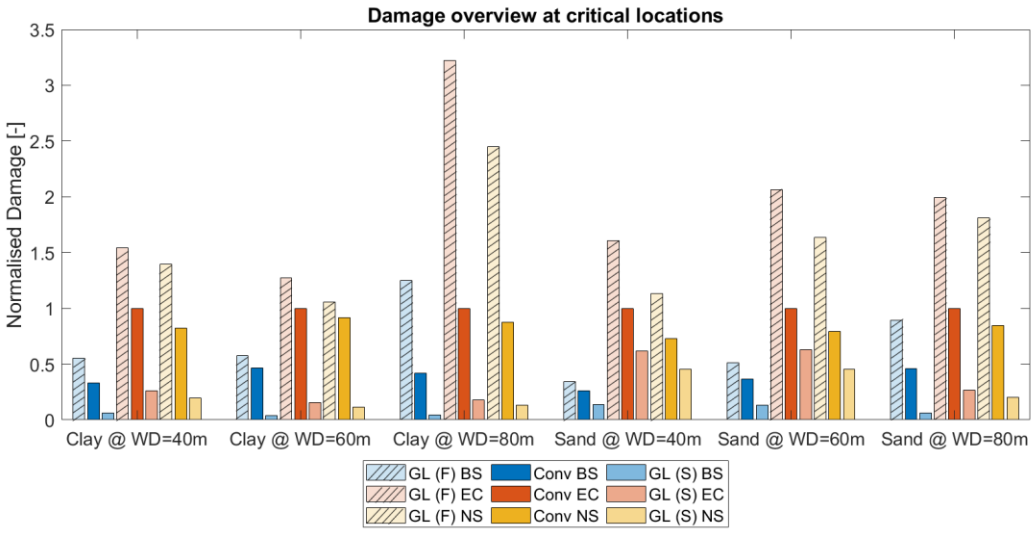

Figure 7-3: Fatigue results of guyed (GL) monopiles with flexible (F) tendons and stiff (S) tendons with respect to the conventional monopile (Conv) fatigue damage considering the 22 MW turbine

Figure 7-3 reveals that flexible tendons always result in higher fatigue damage compared to the conventional monopile, whereas the stiff guyed system shows lower fatigue damage.

The flexible guyed monopile system has a natural frequency similar to that of the conventional monopile, however the bending moment amplitudes are larger. This may be due to the pretension in the tendons, as the magnitude to the amplitudes correlates with the pretension setup in the model. However, this hypothesis has not been confirmed and is considered outside the scope of this thesis.

Conversely the guyed monopile system with stiff tendons demonstrates significant theoretical potential. The high stiffness of the tendons shifts the systems natural frequency outside of the peak spectrum. However, idling contributes more to fatigue damage for the guyed monopile compared to the conventional monopile. This indicates that the wave contribution to the total fatigue damage is higher for the guyed monopiles, a finding that contrasts with the mode shape conclusions. Additionally, the lower fatigue damage in this system may result from the stiffness of the tendons, restricting the vibrations. This results in lower bending moment amplitudes compared to the conventional monopile. This finding requires more research and is therefore recommended for future studies.

7.4.2 Fatigue locations assessment

The subsection above concludes that unfeasible stiff tendons show reduced fatigue damage at the critical location compared to the conventional monopile, whereas tendons with a feasible stiffness show an increase in fatigue damage. These conclusions are based on the analysis at the assumed critical locations of both foundations documented in section 7.3. As mentioned in section 6.5 the conventional monopile dimensions have been optimized by RA. The guyed monopile dimensions are reduced significantly over the length of the monopile, as elaborated on in section 4.3, hence, not optimized based on the structural behavior the guyed monopile system.

This subsection analyzes the fatigue damage of the guyed monopile, using a feasible tendon stiffness, at the critical location (conn) as well as the mudline (ML) compared to the conventional monopile fatigue damage. The results are visualized in Figure 7-4.

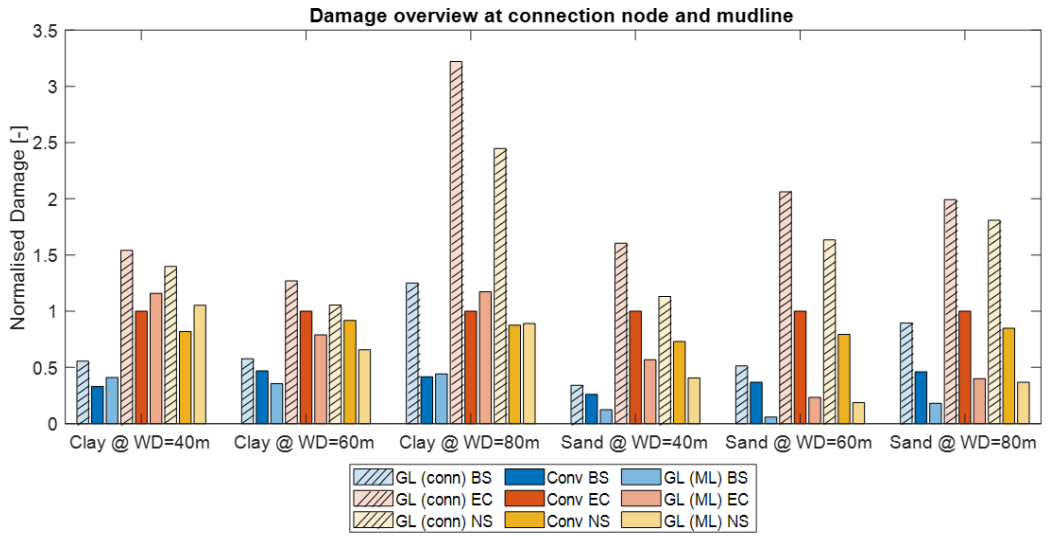

Figure 7-4: Fatigue results of guyed monopiles (GL) with flexible tendons at critical location (conn) and mudline (ML) with respect to the conventional monopile (Conv) fatigue damage considering the 22MW turbine

As concluded in section 7.4.1, the connection node experiences higher fatigue damages compared to the conventional monopile. However, the mudline damage of the guyed monopile is generally lower, with higher values only occurring in clay conditions at water depths of 40 meters and 80 meters. This shows that when considering feasible tendons, the guyed monopile could be beneficial for fatigue when optimizing the guyed structure. The figure suggests strengthening the connection points, the amount of steel could be reduced at the mudline. Additionally, as the connection point is more visually accessible, lower safety factors regarding fatigue can be used compared to the safety factors used at and below mudline. As safety factors and stress concentration factors have been neglected in this research, it has not been further elaborated on. However, this should be considered in future research regarding fatigue and guyed monopile optimization, as this will reduce the amount of steel required at the connection point.

7.4.3 Turbine size

Finally, this section presents the results for the 15MW guyed monopile foundation, considering feasible tendons, the same locations on the foundations are analyzed as in 7.4.2. As in the 22MW guyed monopile analysis, the tendons stiffness is tuned so that the natural frequency of the guyed monopile is equal to the conventional monopile. The results are shown in Figure 7-5, where similar conclusions are found considering the 15MW guyed monopile foundation as for the 22MW guyed monopile foundation documented in section 7.4.2.

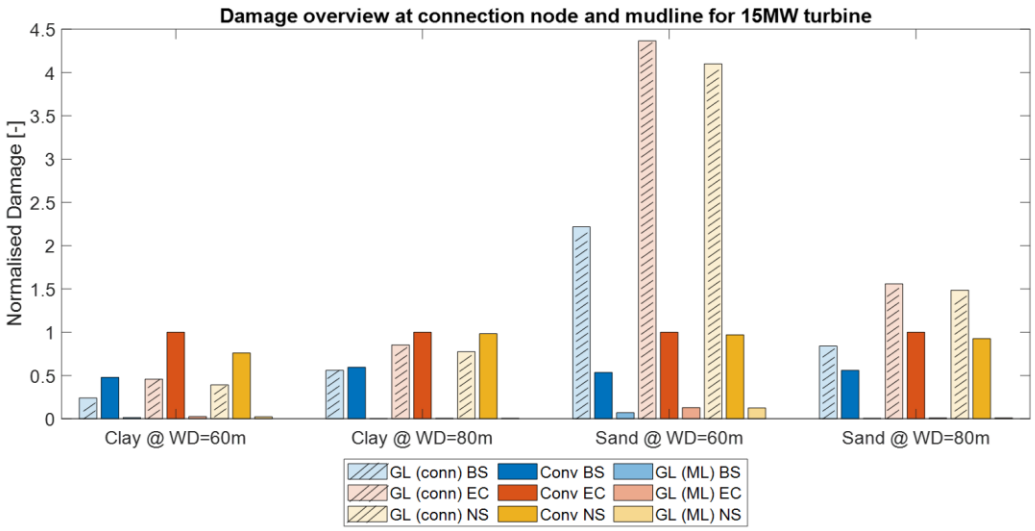

Figure 7-5: Fatigue results of guyed monopiles (GL) with flexible tendons at critical location (conn) and mudline (ML) with respect to the conventional monopile (Conv) fatigue damage considering the 22MW turbine

Figure 7-5 shows that for the guyed monopile in clay conditions, both the connection point and mudline fatigue damage are less compared to the conventional monopile fatigue damage at mudline. In sand conditions, the fatigue damage at the connection point is larger than that of the conventional monopile. A difference compared to the 22MW guyed monopile is the extremely low fatigue damage at mudline for the guyed monopile, suggesting the mass can be reduced more when optimizing the foundation for a guyed system.

7.5 CHECKS

The results above demonstrate the effect of the guyed monopile system on fatigue. For the conventional monopile, the literature reviewed in section 2 concluded that fatigue was the governing design limit state. However, for the guyed monopile, other limit states or failure mechanisms may be governing. The purpose of this section is to provide checks that demonstrate the guyed system compliance with ULS and to elaborates on the risk of snap loads in the tendons.

The same design load cases (DLC) are used in this thesis for both the ULS checks as well as the tendon snap load checks. The design load cases, which correlated with the DLCs documented in DNV [29], are elaborated on below. It is assumed that these loads cases provide a sufficient overview of the performances of the guyed monopile system in terms of ULS and snap loads limitations, as extreme wind and wave conditions are considered in both operational and idling conditions. Furthermore, resonance is analyzed as this leads to large displacement resulting in either snap loads or pile yields.

DLC1 considers operational conditions at rated wind speed (11m/s). For the hydrodynamic forcing, the 50 year joint probability wave height is used in the rated wind speed bin. The corresponding period is estimated from the equation below.

$$11.2\sqrt{\frac{H_s}{g}} \leq T \leq 14.3\sqrt{\frac{H_s}{g}}$$

DLC2 considers extreme conditions during idling. The 50 year wind along with the 5 year wave are used for this analysis and are in accordance with Table 5-2. As shown in the table, only significant wave height data from the MOOD DHI portal can be extracted. In this thesis, the maximum wave height is determined using the following equation.

$$H_{max} = H_s \sqrt{\frac{1}{2} \ln N_w}$$

Where N_w corresponds to the mean zero down crossing period of the sea level elevation and the 1 hour sea-state duration. The corresponding period is estimated in accordance with the equation above.
DLC3 also considers extreme conditions during idling and is similar to DLC2. The difference is, this load case considers the 5 year extreme wind along with the 50 year wave.
DLC4 considers ULS resonance during idling, therefore neglecting the aerodynamic damping at 11m/s wind speed. A JONSWAP wave input with a peak period corresponding to the natural period of the system is used for this load case. Furthermore, the mean significant wave height corresponding to the wind class is used.

As the East Coast of the US has the largest extremes, these environmental values are used for the analysis of all ULS DLC's.

Table 7-1: Design load cases used for USL and snap load checks

	Turbine	$\boldsymbol{U_w}$ $[\boldsymbol{m/s}]$	$\boldsymbol{H_{max}}$ $[\boldsymbol{m}]$	$\boldsymbol{T_p}$ $[\boldsymbol{s}]$
DLC1	Operational	11	8.4	12.9
DLC2	Idling	53.6	10.9	10.4
DLC3	Idling	29.7	20.8	19.5
DLC4	Idling	11	1.6	$1/f_n$

7.5.1 Ultimate Limit State

Regarding ULS, only a yield check has been performed. Both the global buckling and local buckling checks have been neglected as buckling has been extensively researched by Van Doormaal [19], mentioned in section 2.5.

For the yield check, the three dimensional Von Mises criterion can be applied. For a more conservative and simplistic approach, the cross-sectional yield capacity can be checked on the basis of the design value as shown below.

$$\sigma_{x;d} = \left| \frac{F_x}{A} - \frac{M_y}{I_y} + \frac{M_z}{I_z} \right| \leq \frac{f_y}{\gamma_m}$$

Here, f_y is the yield stress and γ_m is the material safety factor. This analysis considers the steel yield stress and the material factor to be 355 MPa and 1.1 respectively. The other parameters have been elaborated on in section 4.2.1. This conservative approach is deemed valid for the purpose of this thesis, as this section only provides checks.

The yield capacity criterion is checked for all three DLC's at the tendon connection node. This node is assumed to be the critical location using the same reasoning as documented in section 7.3.

The results of the ULS checks per DLC are given as a fraction of $\sigma_{x;d}\gamma_m/f_y$ indicating that values larger than 1 do not comply with the yield check criteria. The results are documented in Table 7-2 showing that all DLC's comply with the yield criteria. It is concluded that there is no risk to the foundation when considering these four ULS load cases.

Table 7-2: ULS results for 22 MW guyed monopile foundations

	DLC1	DLC2	DLC3	DLC4
Clay @ 40m WD	0.0825	0.0383	0.0296	0.0275
Clay @ 60m WD	0.0728	0.0360	0.0289	0.0403
Clay @ 80m WD	0.0747	0.0418	0.0294	0.0529
Sand @ 40m WD	0.1080	0.0496	0.0385	0.0558
Sand @ 60m WD	0.0898	0.0424	0.0338	0.0515
Sand @ 80m WD	0.0745	0.0367	0.0288	0.0412

7.5.2 Snap loads

Snap loads are abrupt shifts in tension magnitude along mooring lines or cables. These loads can include shocks on the line material as well as the structure the cable is attached to, significantly diminishing its fatigue life. The magnitude of the snap loads is complex to estimate, therefore, the occurrence of snap loads has been analyzed in this thesis.

This research assumes that snap loads occur after a tendon experiences slack. The tension in the tendon is dependent on the pretension and on the motion of the guyed monopile. A pre-tension in accordance with literature [21] in section 2.5 is assumed, and using data sheets of Dyneema SK99 HMPE ropes.

The results for the DLC's considered in this check are documented in Table 7-3. The results show the ratio $(L_e - L)/(L_e - L_0)$, where L_e and L_0 are the lengths of the line in pretension and slack, respectively. L is the shortest length of the line during the 1 hour DLC simulation. In this simulation, all three lines have been analyzed, and Table 7-3 documents the most severe line. Results larger than 1 indicate the line has been in slack during the simulation, resulting in snap loads. Although no clear relation can be found from these results, it can be concluded that a snap load has occurred during a DLC3 simulation for a 60 meter water depth guyed monopile in a sand profile. Furthermore, the results show that more load cases indicate a line almost being slack, $(L_e - L)/(L_e - L_0) > 0.9$, which highlights the importance of considering snap loads in further design works for guyed monopiles. Finally, other representations of the environmental conditions over a 1 hour period could show more load cases with a snap load occurring.

The DLC's solely show results regarding 50 year return period environmental conditions complying with ULS standards. ALS, considering 100, 1.000, 10.000 year return periods of environmental conditions will result in a higher probability of snap loads snap loads.

To mitigate this risk of a snap load, the pretension of the tendon should be increased. Increasing the tendon stiffness will reduce the motion of the monopile, however, the change in elongation $(L_e - L_0)$ will also decrease. This relationship has not been analyzed in this thesis.

Table 7-3: Snap load results for 22 MW guyed monopile foundations

	DLC1	DLC2	DLC3	DLC4
Clay @ 40m WD	0.5350	0.3472	0.5309	0.6560
Clay @ 60m WD	0.2229	0.6233	0.9194	0.6269
Clay @ 80m WD	0.0164	0.7420	0.8318	0.7558
Sand @ 40m WD	0.6863	0.3150	0.6041	0.6704
Sand @ 60m WD	0.6289	0.6437	1.0873	0.9322
Sand @ 80m WD	0.2419	0.6446	0.9460	0.6621

7.6 General discussion

This section elaborates on the general assumptions made in the methodology and analysis of the guyed monopile system, influencing the conclusions drawn. Regarding the fatigue analysis, reference is made to the discussion section documented in 6.5.

As mentioned in 3.4, OpenFAST uses a linear spring theory to model the tendons. Therefore, the springs apply a reaction force when in tension as well as in compression, the latter isn't feasible in reality. Modelling springs solely working in tension will change the structural properties of the system, potentially having a negative impact on the natural frequency of the guyed monopile system, the total fatigue damage and ULS and snap load checks.

Additionally, this research is based on three tendons equally distributed over the cross-section of the monopile at 10 meters below MSL. To add redundancy, literature suggest two sets of tendons in three directions [21]. This risk mitigation will influence the required size of the tendon as the stiffness of a tendon set has a linear relation when a parallel relation is assumed, $k_{tot} = k_1 + k_2$. Therefore, adding multiple sets of tendons, not only has a positive effect on redundancy, but will also positively influence the structural properties and reduce the costs of the tendons. In contrast, this mitigation adds challenges for installation.

Furthermore, the simulations assume the pretension to be constant throughout the lifetime of the structure. However, due to creep, the tension in the lines will decrease over time. This aspect should be considered as re-tensioning or replacing the tendons is costly. For example, considering the Dyneema SK99 HMPE line, assuming a yearly creep rate of 1% is reasonable based on data sheets. Over the lifetime of 25 years the Dyneema SK99 line will be irreversibly elongated by 28% resulting in slack lines, hence having no positive effect on the structural properties of the guyed monopile system. Using a Dyneema SK20 line for the tendons will mitigate this challenge as this is a creep resistant material with yearly creep rates lower than 0.1%. However, this material has a 30% strength disadvantage compared to the Dyneema SK99.

Finally, this research analyzes two locations on the monopile length regarding fatigue damage, namely the mudline node and the tendon connection node. The latter is based on the critical location assumption, corresponding to the location of the highest mean moment magnitude occurring on the length of the monopile. This assumption is reasonable for conventional monopiles as the initial monopile design optimization tool was used for the monopile dimensions. For the guyed monopile system, the dimensions have been modified and not optimized to show stress amplitudes similar to those of the conventional monopile. Analyzing the fatigue damage at the mudline as documented in sections 7.4.2 and 7.4.3 showed

lower fatigue damages occurring at mudline. Therefore, optimizing the guyed monopile foundation will results in different foundation dimensions and masses than those considered in this research.

Despite these limitations, the primary goal is to analyse the potential of guyed monopile systems in terms of fatigue analysis. Therefore, the conclusions drawn can still be considered valid.

8 CONCLUSION & RECOMMENDATIONS

This master thesis applies an existing and verified frequency domain fatigue damage estimation methodology, which couples aerodynamic and hydrodynamic excitations and incorporates blade passing frequency excitations to the method. Using this methodology helps answer the research questions: ***How do different geographical regions impact the fatigue of a monopile (RQ1) and how can guyed monopile systems help design and operate monopiles in deeper/harsher operational conditions? (RQ2)***

The proposed methodology estimates the fatigue damage on XXL monopiles by using the joint probability of wind and waves, taking into account both directionality and misalignment. The frequency domain method uses a transfer function from wave elevation to stress response. The stress transfer function uses input from shear forces and bending moments. These are estimated by the integrated load analysis tool OpenFAST, which couples aerodynamics, hydrodynamics, structural dynamic and control systems. The input forces and moments are determined by assuming 1 hour wave noise wave excitation and uniform wind, as per a given scatter diagram. The conventional XXL monopile dimensions have been optimized for three water depths and two soil parameters using an initial monopile design tool and the IEA 22MW and IEA 15MW reference turbines. Fatigue calculations have been performed for the Baltic Sea, East Coast of the United States and the North Sea Coast of Denmark using metocean hindcast data from the MOOD DHI Portal as input, in accordance with the frequency domain methodology. Only operational wind conditions, ranging from 3 to 25 m/s, along with the joint probabilities of waves are used to estimate the operational fatigue as well as the idling fatigue. The conclusions derived from these estimates are documented in section 8.1.

Additionally, the effect of implementing guyed lines to the monopile has been analysed, by modelling the tendons as linear springs in OpenFAST. The benefit of weight reduction has been achieved by reducing the diameter of the conventional monopile. Furthermore, multiple stiffness and tendon configurations have been analysed visualising the effects of these parameters. Finally, this thesis introduces novel insights regarding the fatigue analysis leading to conclusions documented in section 8.2.

8.1 CONVENTIONAL MONOPILE FATIGUE ANALYSIS

How do different geographical regions impact the fatigue of a monopile?

This research concludes that the placement of the structure's natural frequency in the wave spectrum dominates fatigue damage. Geographical regions with the highest energy density of waves in line with the natural frequency of the system show the highest fatigue damage, especially for cases with low aerodynamic damping, which mainly occurs in the fore aft direction. These cases have a higher impact on the fatigue damage, whereas the directional spreading of wind and waves has less influence.

Three cases with low aerodynamic damping are considered in this research. First, aerodynamic damping depends on the rotational speed of the rotor, with higher rotational speeds resulting in higher aerodynamic damping. Wind speeds below the rated wind speed, which in this research is lower than 11 m/s, have lower rotational speeds, resulting in lower aerodynamic damping. Therefore, when solely considering wind-wave alignment, the fatigue damage in the US East Coast region, experiencing lower wind speeds, was higher compared to the North Sea, even though the wave energy density spectra are similar. Secondly, idling has a significant contribution to fatigue damage. This research assumes a realistic

idling period during operational conditions. This idling period contributes to 70% fatigue damage in shallow water and a 50% contribution in deep water for a 22MW turbine. This difference is predominantly dominated by a form of hydrodynamic damping, which is higher in deeper waters. In the North Sea and US East Coast regions, lower contributions to fatigue damage due to idling is concluded for the 15MW turbine, compared to 22MW turbine, as the natural frequency of the 15MW system is higher and therefore shifted to a lower part of the wave energy density spectrum. In the Baltic Sea, a higher idling contribution to fatigue damage is found for the 15MW turbine, as the natural frequency shifted to the peak wave energy density frequency. Thirdly, this research shows that wind-wave misalignment has significant impact on fatigue damage. Wind-wave misalignment cases can occur up to 60% of the lifetime of the wind turbine for the geographic location considered. Including these misalignment factors, according to the frequency domain methodology used in this research, can result in an increased fatigue damage of 400% compared to only considering wind-wave alignment. This increase is dependent on the wind-wave misalignment angle, as higher misalignment angles show higher fatigue damages, and the placement of the natural frequency in the wave energy density spectrum.

The significant increase in fatigue damage when considering wind-wave misalignment originates from the choice to model wind as uniform in this thesis. Modelling the wind as uniform, linearizes the stress output, making it solely dependent on the hydrodynamic excitations whilst including aerodynamic effects. However, the modelling choice to neglect turbulence in wind, underestimates the fatigue damage for aligned waves and slightly misaligned waves. This results in fatigue damage being dominated by wind-wave misalignment cases. Including turbulence increases the fatigue damage of aligned waves and slightly misaligned waves. Hence, including turbulence results in less pronounced fatigue damage differences in the US East Coast and North Sea regions and likely a higher influence of wind-wave directional spreading on fatigue. Uniform wind and turbulent wind both show an increase in magnitude of fatigue damage with an increasing misalignment angle. Therefore, assuming a uniform wind provides reasonable results in identifying differences in fatigue damage caused by geographical metocean conditions, thereby answering the research question.

8.2 GUYED MONOPILE

How can guyed monopile systems help design and operate monopiles in deeper/harsher operational conditions?

Adding guyed lines to a monopile alters the structural properties of the foundation by increasing stiffness and stability and transferring a significant part of the excitation loads directly to the soil. Therefore, the guyed line monopiles can be designed lighter compared to conventional monopiles. This dimension reduction strategy results in a significant weight reduction for 15MW guyed monopile foundations in 80 meter water depths and similar weight reduction percentages for the 22MW guyed monopile foundations in 60 and 80 meter water depths.

Reducing the amount of steel used in monopiles results in a more compliant structure, with the system's overall stiffness being influenced by the stiffness of the tendons. Higher tendon stiffness results in higher natural frequencies of the guyed monopile. In clay soil conditions, the natural frequency envelope of guyed monopile systems is broader compared to those in sand soil conditions. Similarly, deeper waters, as well as larger turbines contribute to a larger natural frequency envelope. Finally, among various tendon line configurations, connecting the tendons at mean sea level resulted in the largest natural frequency

envelope. However, to mitigate safety hazards caused by this configuration, the base case in this thesis assumes that the tendons are connected at 10 meters below mean sea level.

Additionally, the tendons change the mode shapes but do not significantly influence the frequencies exciting the second mode compared to the conventional monopile. The change in mode shape is correlated to the stiffness of the tendon, where the initial tension of the tendon has little influence. An increase of tendon stiffness shows a decrease in wave energy transferred to the foundation compared to the conventional monopile regarding the first two mode shapes. Due to OpenFAST limitations, higher mode shapes could not be analysed and soil structure interaction has been neglected in the mode shape.

Finally, changing the dimensions and the structural properties of the foundations affects the fatigue damage. The fatigue damage analysis on the 22MW guyed monopile foundations show lower fatigue damages at the critical location, in this research assumed to be at the tendon connection point, compared to the conventional monopile using ultra stiff tendons. This extreme tendon stiffness is deemed technically unfeasible. A feasible tendon stiffness resulting in similar natural frequencies to the conventional monopile, showed higher fatigue damage compared to the conventional monopile at the critical locations. Analysing the fatigue damage at the mudline of the guyed monopile shows lower fatigue damages than the conventional monopile. Similar results were found for the 15MW guyed monopile foundations, indicating that the assumed mass reduction strategy for guyed monopiles needs to be further optimized. Some critical locations of the guyed monopile may require strengthening, whereas other locations on the pile may require less steel.

Hence, the results demonstrate the technical potential of the guyed monopile system, particularly when the foundation is optimized based on the structural properties to ensure lighter foundations in deeper waters. However, a potential showstopper is the risk of snap loads, which requires further analysis and is recommended to be performed using a different software due to OpenFAST limitations. Elaboration on this recommendation along with further recommendations for future research are elaborated on in section 8.3.

8.3 Recommendations

While the findings in this thesis help fill gaps in the literature, they also highlight areas for future research. The recommendations are devided into three categories namely, the general recommendations focussing on the model, conventional monopile recommendations and guyed monopile recommendations. An author's opinion is provided on if the methodology and software tool used in this research are applicable for the future research points.

8.3.1 General

As discussed, OpenFAST V3.5.0 has shortcomings regarding fatigue analysis as wave diffraction has been neglected. The inclusion of diffraction will have a positive impact on the fatigue life of monopile structures, particularly those in regions with short waves. Furthermore, OpenFAST V3.5.0 neglects soil structure interaction, disregarding the highest damping factor after aerodynamic damping of the system. Including this effect will result in lower fatigue damages for wind-wave misalignment cases and potentially making wind-wave directionality more governing. Therefore, it is recommended to conduct the same methodology analysis using input loads form OpenFAST V4.0 which include the effects of diffraction and soil damping.

Additionally, analysing of mode shapes in OpenFAST is challenging due to the Rayleigh damping formulation built in the tool. Furthermore, the mode shapes disregard the effect of soil structure interaction which will influence the mode shapes. Therefore, it is recommended to do mode shape and modal frequency analysis using a different tool.

8.3.2 Conventional monopile

The results regarding the conventional monopile show the fatigue damage is governed by the alignment of the peak wave frequency and the natural frequency of the monopile. The fatigue damage is calculated using a 1 hour white noise wave spectrum. Therefore, the period of wave frequencies that excite the natural frequency is relatively short. Hence, it is recommended to perform full JONSWAP simulations with a wave peak period aligning with the natural frequency investigating the effect of long resonance periods with respect to fatigue (FLS) and yield (USL). For this investigation, the methodology used in this thesis does not comply however, the OpenFAST model used in this thesis and a time domain fatigue post processing tool will give relevant findings regarding resonance effect on fatigue and yield.

Furthermore, the methodology used for this research assumes uniform wind, analysing the differences in fatigue damage from the wave scatter. The thesis also shows that turbulence significantly contributes to aligned wind-wave fatigue damage. Geographical regions differ not only have in metocean wave conditions, but also in turbulence intensities. Therefore, it is recommended to do a fatigue damage assessment focussing on the turbulence intensities occurring in the geographical regions. The frequency domain fatigue damage estimation methodology in this research does not include turbulent winds, making it not useful for this analysis. This analysis requires time domain simulations. To avoid full time domain integrated load simulations over the full scatter diagram the lumping method developed by Katsikogiannis et al. [23] is recommended. For the input loads, OpenFAST is recommended as this integrated load analysis tool is highly advanced in aerodynamic loading. Therefore, including turbulence to this model will provide relevant load responses to be used in the time domain fatigue damage methodology.

8.3.3 Guyed monopile

As mentioned in section 8.2, the most significant obstacle for the guyed monopile system is the risk of snap loads and the consequences of such an event. The ability of performing this analysis in OpenFAST is low, as the modules are not able to plot the tensions in the tendon line over time. Therefore, this research assumes that snap loads occur when the distance between the connection node on the monopile and the soil node is shorter than the length of the tendon in slack conditions. Additionally, the point load at the connection point, resulting from a snap load cannot be analysed in OpenFAST. Hence the magnitude of the snap load in the tendon and the effect on monopile fatigue cannot be analysed in OpenFAST. For further research it is recommended to estimate snap loads using other software tools, for example OrcaFlex, considering multiple load cases. Interface loads at the tower base can be used from OpenFAST and integrated into OrcaFlex for the snap load analysis.

In addition, OpenFAST can only model the tendons as linear springs working in both tension and compression. However, the total stiffness according to this assumption is over estimated. Modelling the tendons as springs only working in tension will change the structural properties of the system influencing the fatigue life. Hence, it is recommended to analyse how modelling springs solely in tension affects the fatigue life of the system. This analysis can also be performed in OrcaFlex, where again the tower base interface loads can be integrated from OpenFAST.

Furthermore, this research utilizes a dimension reduction strategy based on an optimized conventional monopile. However, as shown the guyed monopile system has different structural properties compared to the conventional monopile leading to different critical locations regarding fatigue damage. Including soil structure interaction using OpenFAST V4.0 will give insights on how the loads are distributed into the soil. These results give input for an optimization tool, giving valuable insights on the dimension reduction strategy. Additionally, the potential of decreasing the embedment length of the guyed monopile compared to the conventional monopile can be analysed and optimized. Therefore, it is recommended to build a preliminary optimization tool, based on the methodology used in this research and the OpenFAST V4.0 tool to verify conclusions based on mass reductions. This optimization should be performed using the appropriate safety factors.

Finally, it is concluded that for tendons with a feasible stiffness for the 15MW and 22MW turbines, higher fatigue damages occur at the critical locations compared to the conventional monopile under the assumed diameter reduction strategy. Analysing the time domain moments show amplitudes in the same order of magnitude as the pretension. Therefore, it is recommended to analyse the effect of the pretension on the response forces around the connection point. This can be analysed using the OpenFAST model used for this research.

NOMENCLATURE

Abbreviations

ALS	Accidental limit state
DLC	Design load case
FA	Fore aft direction (*In line with the rotor plane*)
FFT	Fast Fourier Transform
FLS	Fatigue limit state
IEA	International Energy Agency
MSL	Mean sea level
OWT	Offshore wind turbine
SCD	Scatter diagram
Shell	Shell Global Solutions International B.V.
SLS	Serviceability limit state
SS	Side-side direction (P*erpendicular to the rotor plane*)
SSI	Soil structure interaction
ULS	Ultimate limit state
XXL monopile	Monopile diameters > 9 meter

BIBLIOGRAPHY

[1] DNV, “Energy Transition Outlook 2022,” DNV, Hovik, 2022.

[2] J. K. Kaldellis and M. Kapsali, “Shifting towards offshore wind energy-Recent activity and future development,” *Energy Policy,* vol. 53, pp. 136-148, 2013.

[3] X. Wu, Y. Hu, Y. Li, J. Yang and et.al, “Foundations of offshore wind turbines: A review,” *Renewable and Sustainable Energy Reviews,* vol. 104, pp. 379-393, 2019.

[4] Wind Europe, “Wind energy in Europe in 2019 - trends and statistics,” Wind Europe, Brussels, 2020.

[5] K. W. Hermans and J. M. Peeringa, “Future XL monopile foundation design for a 10 MW wind turbine in deep water,” ECN-E--16-069, 2016.

[6] S. Sanchez, J. S. Lopez-Guitierrez, V. Negro and M. Dolores Esteban, “Foundations in offshore wind farms: Evolution, characteristics and range of use. Analysis of main dimensional parameters in monopile foundations,” 2019.

[7] U. D. o. Energy, “Offshore Wind Market Report,” Offshore of Energy Efficiency & Renewable Energy, 2022.

[8] L. Arany, S. Bhattacharya, J. H. Macdonald and S. J. Hogan, “Closed form solution of Eigen frequency of monopile supported offshore wind turbines in deeper waters incorporating stiffness of substructure and SSI,” *Soil Dynamics and Earthquake Engineering,* vol. 83, pp. 18-32, 2016.

[9] L. Wang, A. Kolios, X. Liu, D. Venetsaons and R. Cai, “Reliability of offshore wind turbine support structures: A state-of-the-art review,” *Renewable and Sustainable Energy Reviews,* p. Volume 161, 2022.

[10] B. Yeter, Y. Garbatov and C. G. Soares, “Fatigue reliability of an offshore wind turbien supporting structure accounting for inspection and repair.,” in *Analysis and Design of Marine Structures*, CRC Press, 2015, pp. 751-762.

[11] J. Velarde and E. E. Bachynski, “Design of fatigue analysis of monopile foundations to support the DTU 10 MW offshore wind turbine,” *Energy Procedia,* vol. 137, pp. 3-13, 2017.

[12] W. Njomo Wandji, A. Natarajan and D. N. Krasimirov, “Influence of model parameters on design of large diameter monopiles for multi-megawatt offshore wind turbines at 50-m water depths,” *Wind Energy,* 2017.

[13] IEA, “Offshore Wind Outlook 2019: World Energy Outlook Special Report,” International Energy Association,, Paris, 2019.

[14] V. Laface, G. Alotta, G. Failla, C. Ruzzo and F. Arena, “A two-degree-of-freedom tuned mass damper for offshore wind turbines on floating spar supports,” *Marine Structures,* vol. 83, 2022.

[15] H. Zuo, K. Bi and H. Hao, “Using multiple tuned mass dampers to control offshore wind turbine vibrations under multiple hazards,” *Engineering Structures,* vol. 141, pp. 303-315, 2017.

[16] M. L. Brodersen, A. Bjørke and J. B. Høgsberg, “Active tuned mass damper for damping of offshore wind turbine vibrations,” *Wind Energy,* vol. 20, pp. 783-796, 2017.

[17] J. Van der Ploeg, “Perforation of Monopiles to Reduce Hydrodynamic Loads and Enable use in Deep Waters,” Technical University of Delft, 2021.

[18] G. A. Santamaria Gonzalez, “Advantages and Challenges of Perforated Monopiles in Deep Water Sites: Comprehensive study of stress concentrations and fatigue loads of monopile foundations in deep water sites,” Technical University Delft, 2023.

[19] T. Van Doormaal, “Conceptual analysis on Guyed Monopiles for Offshore Wind Turbine Generators in Deep Water,” Technical University Delft, 2023.

[20] M. Antoniou, F. Gelagoti and I. Anastasopoulos, “A compliant guyed system for deep-sea installations of offshore wind turbines: Concept, design insights and dynamic performance,” *Soil Dynamics and Earthquake Engineering,* vol. 119, pp. 235-252, 2019.

[21] M. Jespersen and U. S. Andersen, “Guyed Wind Turbine Towers,” in *Nordic Steel*, Copenhagen, 2019.

[22] “IEAWindTask37 respository,” [Online]. Available: https://github.com/IEAWindTask37.

[23] G. Katsikogiannis, S. H. Sorum, E. E. Bachynski and J. Amdal, “Environmental lumping for efficient fatigue assessment of large-diameter monopile wind turbines,” *Marine Structures,* vol. 77, no. 102939, 2021.

[24] M. N. Scheu, L. Tremps, U. Smolka, A. Kolios and A. Brennan, “A systematic failiure mode effects and criticality analysis for offshore wind turbine systems towards integrated condition based maintenance strategies,” *Ocean Engineering,* vol. 176, pp. 118-133, 2019.

[25] M. Martinez-Luengo and M. Shafiee, “Guidlines and cost-benefit analysis of the structural health monitoring implementation in offshore wind turbine support structures,” *Energies,* vol. 12, no. 1176, 2019.

[26] DNV, “Support structures for wind turbines (DNV-ST-0126),” DNV, Hovik.

[27] L. Arany, S. Bhattacharya, J. Macdonald and J. Hogan, “A critical review of serviceability limit sate requirements for monopile foundations of offshore wind turbines,” in *Offshore Technology Conference*, Houston, 2015.

[28] S. Bhattacharya, "Challenges in design of foundations for offshore wind turbines," *Engineering & Technology reference,* vol. 9, pp. 1-9, 2014.

[29] DNV, "Offshore standard DNV-OS-J103," Design of Floating Wind Turbine Structures, 2013.

[30] M. Orlando, J. Ligthart, J. Van Wijk and M. Schaap, "Pile installation fatigue damage from impact driving records -A case study of offshore monopiles," in *Conference on Foundation Decarbonization and Re-use*, Amsterdam, 2023.

[31] DNV, "DNV-ST-N001," DNV, 2020.

[32] D. J. Salzmann and J. Van der Tempel, "Aerodynamic damping in the design of support structures for offshore wind turbines," in *Offshore Wind Energy Conference*, Copenhagen, 2005.

[33] C. Koukoura, A. Natarajan and A. Vesth, "Identification of support structure damping on full scale offshore wind turbine in normal operation," *Renewable Energy,* pp. 882-895, 2015.

[34] F. N. Santos, N. Noppe, W. Weijtjens and C. Devriendt, "Results of fatigue measurement campaign on XL monopiles and early predictive models," *Journal of Physics:: Confrence Series,* no. 032092, p. 2265, 2022.

[35] J.-T. Horn, J. R. Krokstad and B. J. Leira, "Impact of model uncertainties on the fatigue reliability of offshore wind turbines," *Marine Structures,* vol. 64, pp. 174-185, 2019.

[36] Z. Zha, Y. Lai, S. Rui and Z. Guo, "Fatigue life analysis of monopile-supported offshore wind turbines based on hyperplastic ratcheting model," *Applied Ocean Research,* vol. 136, no. 103595, 2023.

[37] W. Carswell, J. Johansson, F. Løvholt, S. R. Arwade, C. Madhus, D. J. DeGroot and A. T. Myers, "Foundation damping and the dynamics of offshore wind turbine monopiles," *Renewable Energy,* vol. 80, pp. 724-736, 2015.

[38] M. Damgaard, L. V. Andersen and L. B. Ibsen, "Dynamic response sensitivity of an offshore wind turbine for varying subsoil conditions," *Ocean Engineering,* vol. 101, pp. 227-234, 2015.

[39] C. Devriendt, P. J. Jordaens, G. De Sitter and P. Guillaume, "Damping estimation of an offshore wind turbine on a monpile foundation," in *EWEA Conference*, Copenhagen, 2012.

[40] R. Xi, X. Du, P. Wang, C. Xu, E. Zhai and S. Wang, "Dynamic analysis of 10 MW monopile supported offshore wind turbine based on fully coupled model," *Ocean Engineering,* vol. 234, 2021.

[41] J. Van der Tempel, M. B. Zaaijer and H. Subroto, "The effect of scour on design of offshore wind turbines," in *Proceeding of Marec*, 2004.

[42] R. Rezaei, P. Duffour and P. Fromme, "Scour influence on the fatigue life of operational monpile supported offshore wind turbines," *Wind Energy,* vol. 21, pp. 683-696, 2018.

[43] G. E. Varelis, J. Ai, P. Kane, H. Ragheb and E. Dib, "Scour Effects on the Structural Integrity of Offshore Wind Turbine Monopiles," in *3rd International Offshore Wind Technical Conference*, ASME, 2021.

[44] J. Van der Tempel, "Design of support strucure for offshore wind turbines," Delft University of Technology, 2006.

[45] C. M. Fontana, W. Carswell, S. R. Arwade, D. J. DeGroot and A. T. Myers, "Sensitivity of the dynamic response of monopile-supported offshroe wind turbines to structural and foundation damping," *Wind Engineering,* vol. 39, pp. 609-628, 2015.

[46] E. Marino, A. Giusti and L. Manuel, "Offshore wind turbine fatigue loads: the influence of alternative wave moddeling for different turbulent and mean winds," *Renewable Energy,* vol. 102, pp. 157-169, 2017.

[47] B. M. Ayyub, I. A. Assakkaf, D. P. Kihil and M. W. Siev, "Reliability based design guidlines for fatigue of ships structures," *Naval Engineers Journal,* vol. 114, no. 2, pp. 112-138, 2008.

[48] IEC, "Wind energy generation systems-Part 1: design requirements," in *IEC International Standard:61400-1 fourth edition*, Switzerland, International Electrotechnical Commision (IEC), 2019.

[49] T. L. Anderson, "Fracture Mechanics: Fundementals and Applications: Fourth Edition," CRC Press, 2017.

[50] D. Broek, "Elementary engineering fracture mechanics," *Springer Science & Buisiness Media,* 2012.

[51] W. Dong, T. Moan and Z. Goa, "Fatigue reliability analysis of jacket support structure for offshore wind turbines considering the effect of corrosion and inspection," *Reliability Engineering & System Safety,* vol. 106, pp. 11-27, 2012.

[52] DNVGL, "DNVGL-RP-C203: Fatigue design of offshore steel structures," *DNVGL,* 2016.

[53] S. H. Sørum, J. Krokstad and J. Amdahl, "Wind-wave directional effects on fatigue of bottom-fixed offshore wind turbine," in *Joural of Physiucs conference series: IQP*, 2019.

[54] F. Wilberts, "Measurement driven fatigue assessment OF offshore wind turbine foundations," 2017.

[55] M. Miner, "Cummulative fatigue damage," *Journal of Applied Mechanics,* vol. 12, pp. 154-164, 1945.

[56] J. Velarde, C. Kramhoft, J. D. Sorensen and G. Zorzi, "Fatigue reliability of large monopiles for offshore wind turbines," *International Journal of Fatigue,* vol. 134, p. 105487, 2020.

[57] S. Najem Clarke, D. W. Goodpasture, R. M. Bennett, J. H. Deatherage and E. G. Burdette, "Effect of cycle counting methods on effective stress range and number of stress cycles for fatigue prone details," *Transport Research Record,* pp. 49-60, 2000.

[58] G. Marsh, C. Wignall, P. R. Thies, N. Barltrop, A. Incecik and V. Venugopal, "Review and application of Rainflow residue processing techniques for accurate fatigue damage estimation," *International Journal Fatigue,* vol. 82, pp. 757-765, 2016.

[59] S. H. Sørum, "Uncertainties in the design of monopile offshore wind turbines," Doctoral thesis at NTNU, 2023.

[60] J. The and H. Yu, "A critical review on the simulations of wind turbine aerodynamics focusing on hybrid RANS-LES methods," *Energy,* vol. 138, pp. 257-289, 2017.

[61] L. Wang, X. Liu, N. Renevier, M. Stables and G. M. Hall, "Nonlinear aeroelastic modelling for wind turbine blades based on blade element momentum theory and geometrically exact beam theory," *Energy,* vol. 76, pp. 487-501, 2014.

[62] M. Hansen, Aerodynamics of Wind turbines, 2nd edition, London: Routledge, 2007.

[63] T. Burton, N. Jenkins, D. Sharpe and E. Bossanyi, Wind Energy Handbook 2nd edition, Wiley Hoboken, 2011.

[64] J. R. Morison, J. W. Johnson and S. A. Schaaf, "The force exerted by surface waves on piles," *J Pet Technol,* vol. 2, pp. 149-154, 1950.

[65] R. C. MacCamy and R. A. Fuchs, "Wave forces on piles: a diffraction theory," *Army Corps of Engrs,* vol. 69, 1954.

[66] A. N. Robertson, F. Wendt, J. Jonkman and e. al., "OC5 Project Phase Ib: Validation of Hydrodynamic loading on Fixed, Flexible Cylinder for Offshore Wind Applications," *Energy Procidia,* vol. 94, pp. 82-101, 2016.

[67] D. Z. Ning, J. Zang, S. X. Liu, R. E. Taylor, B. Teng and P. H. Taylor, "Free-surface evolution and wave kinematics for nonlinear uni-directional focused wave groups," *Ocean Engineering,* vol. 36, pp. 1226-1243, 2009.

[68] L. Chen, J. Zang, P. H. Taylor, G. Morgan, J. Grice, J. Orszaghova and M. T. Ruiz, "An experimental decomposition of nonlinear forces on a surface-piercing column: Stokes-type expansions of the force harmonics," *Fluid Mechanics,* vol. 833, pp. 773-805, 2018.

[69] DNV, "Bladed Engineering feature summary," DNV.

[70] DTU, "About HAWC2," DTU, [Online]. Available: https://www.hawc2.dk/about-hawc2. [Accessed November 2023].

[71] NREL, “OpenFAST user documentation,” NREL, [Online]. Available: https://openfast.readthedocs.io/en/main/source/user/index.html. [Accessed November 2023].

[72] OrcaFlex, “orcaflex for offshore wind,” Orcina. [Online]. [Accessed November 2023].

[73] IFE Wind Energy Department, “3DFloat-integrated wind turbine simulation software,” IFE, [Online]. Available: https://ife.no/en/service/3dfloat/. [Accessed November 2023].

[74] J. Jonkman and W. Musial, “Offshore Code Comparison Collaboration (OC3) for IEA Tast 23 Offshore Wind Technology and Deployment,” NREL, 2010.

[75] M. Kühn, Dynamics and design optimisation of offshore wind energy conversion systems, Delft: Technische Universiteit Delft, 2001.

[76] M. Seidel, “Wave induced fatigue loads loads on monopiles - new approacheds for lumping of scatter tables and site specific interpoloation of fatigue loads,” in *IWEC*, Hamburg, 2014.

[77] P. Passon, “Damage equivalent wind-wave correlations on basis of damage contour lines for fatigue desing of offshore wind turbines,” *Renewable Energy,* vol. 81, pp. 723-736, 2015.

[78] DNV-GL, “Environmental conditions and environmental loads (DNVGL-RP-C205,” DNV, 2019.

[79] E. Laverton, “Modelling of Metocean Conditions for the Purpose of Planning Marine Operatations,” Mater Thesis NTNU, Trondheim, 2015.

[80] J.-T. Horn, E. Bitner-Gregersen, J. Krokstad and et.all, “A new combination of conditional environmental distributions,” *Applied Ocean Research,* vol. 73, pp. 17-26, 2018.

[81] N. D. P. Barltrop, A. J. Adams and M. G. Hallam, Dynamics of fixed marine structures, London: Butterworth-Heinemann, 1991.

[82] P. H. Wirshing and M. C. Light, “Fatigue under wide band random loading,” *Struct. Div ASCE,* pp. 1593-1607, 1980.

[83] G. K. Chaudhury and W. D. Dover, “Fatigue analysis of offshore platforms subject to sea wave loading,” *International Jounal Fatigue,* vol. 7, 1985.

[84] J. W. Hancock and D. S. Gall, “Fatigue under narrow and broad band stationary loading,” Marine Technology Dirctorate, 1985.

[85] T. Dirlik, “Application of computers in fatigue analysis,” University of Warwick PhD Thesis, 1985.

[86] L. H. Holthuijsen, Waves in Oceanic and Coastal Waters, Cambridge: Cambridge University Press, 2007.

[87] DNVGL-C101, “Design of offshroe steel structures, general,” DNV, 2023.

A LITERATURE REVIEW STRATEGY

This section provides the literature search strategy, giving insight on how relevant literature is found. The literature survey aimed to provide knowledge on fatigue calculations and identification of a research gap.

Certain knowledge on fatigue calculation was obtained in courses during the master Offshore & Dredging Engineering at the Technical University of Delft. This knowledge is used as a starting point. In addition, Google and Google Scholar were used to search for relevant literature. As input for google scholar, the following search words were used:

- Offshore wind turbine support structure
- Monopile
- Limit state
- Fatigue
- Data lumping
- Integrated load tools
- Aerodynamic
- Hydrodynamic
- State of the art review

Furthermore, 2018-2023 was introduced as period to filter the search. To determine relevance, the abstract and conclusions were read. When deemed relevant the paper was read and citations were filtered of relevance by the method introduced above.

It is unfeasible to read all papers on fatigue of offshore wind support structures in a two month time span. Therefore, it is possible the author has missed relevant literature. This section is therefore only a guidance on how the author performed his literature review. The author concludes he has found relevant up to date literature on the subject and has documented everything to the best of his knowledge in section 2.

B NON-NORMALIZED FATIGUE RESULTS

The non-normalised fatigue results are shown in the figure below. Note that these results are based on the assumptions mentioned in the methodology, section 4 and do not include safety factors.

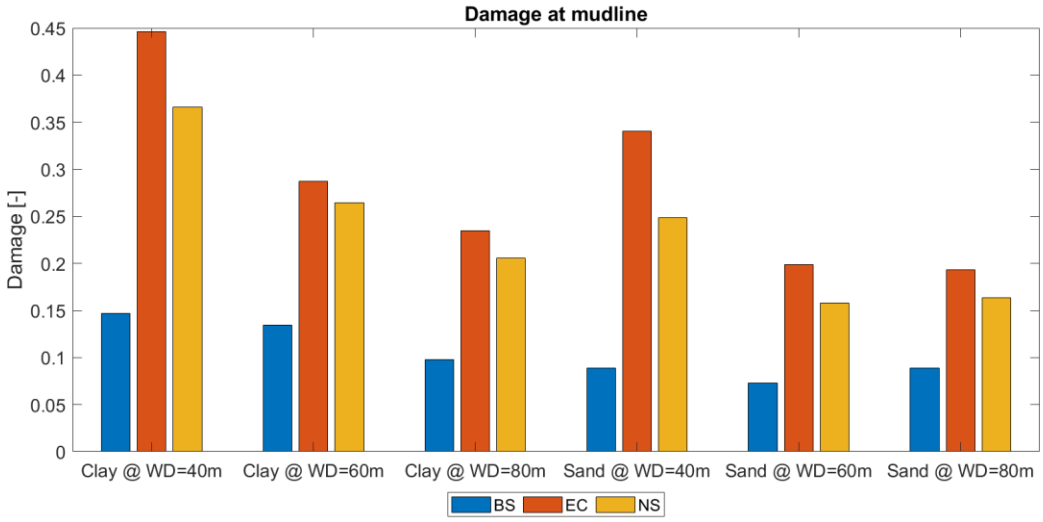

Figure B-0-1: Non-normalized fatigue results for the 22MW turbine

C FATIGUE RESULTS FOR 15MW TURBINES

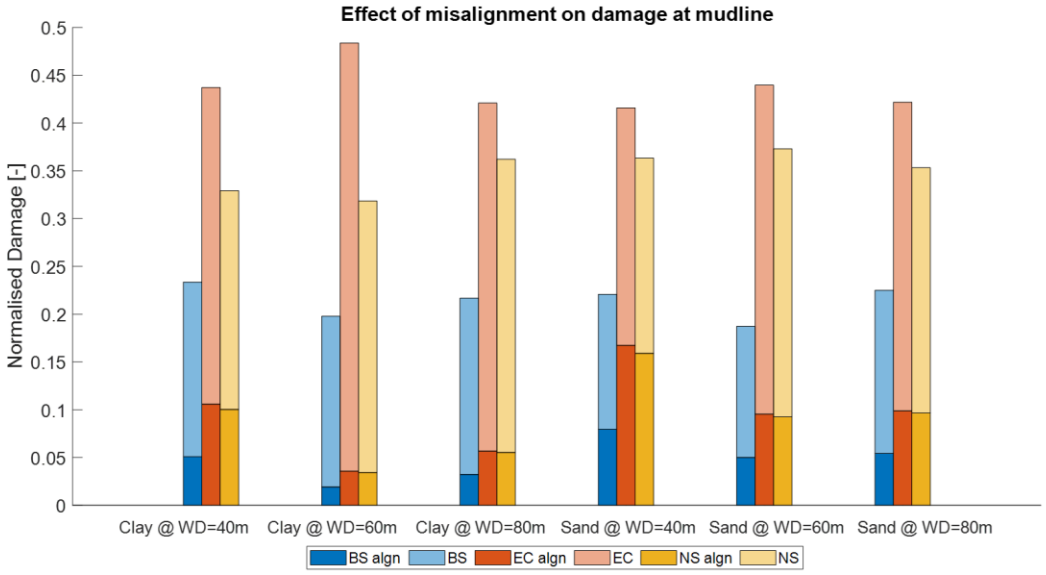

Figure C-0-1: Normalized wind-wave misalignment fatigue results at muddling compared to fully aligned wind-wave conditions for all regions, water depths and soil parameters considering the 15MW turbine

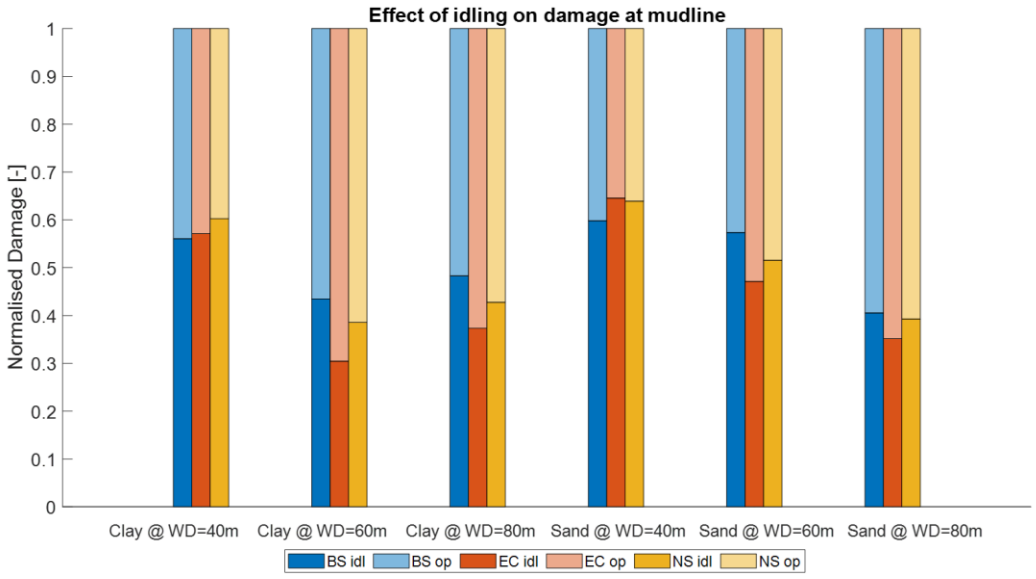

Figure C-0-2: Operational and idling nomalized fatigue results for all regions, water depths and soil parameters considering the 15MW turbine

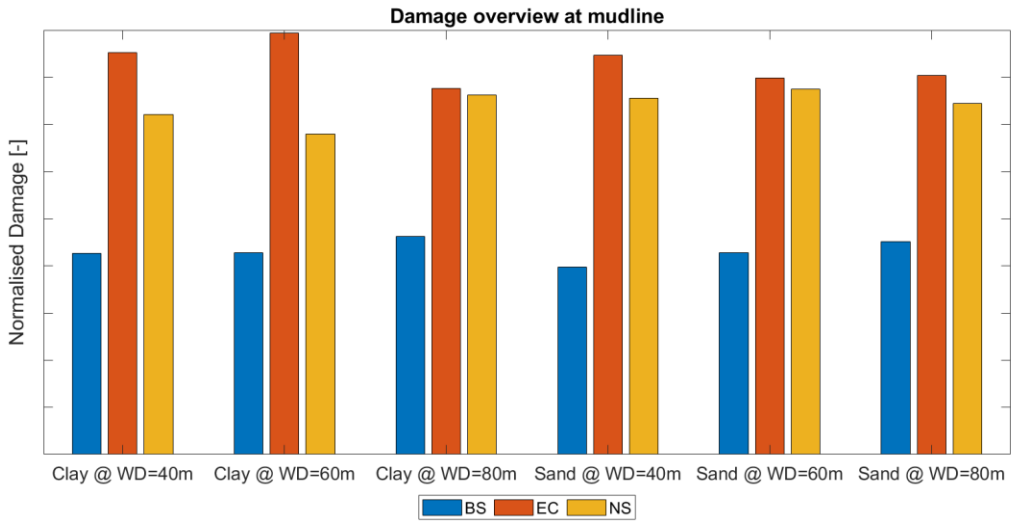

Figure C-0-3: Normalized fatigue results for all water depths and soil parameters considering the 15 MW turbine

D TENDON STIFFNESS AND NATURAL FREQUENCY CORRELATION

E DIAMETERS DYNEEMA SK99 TENDON